Effect of Substrate Temperature on Pattern Formation of Bidispersed Particles from Volatile Drops

Maryam Maria Parsa, Souad Harmand, Khellil Sefiane, Maxence Bigerelle, Raphaël Deltombe

Article

Effect of Substrate Temperature on Pattern Formation of Bi-Dispersed Particles from Volatile Drops

Maryam Parsa, Souad Harmand, Khellil Sefiane, Maxence Bigerelle, and Raphaël Deltombe

J. Phys. Chem. B, **Just Accepted Manuscript** • DOI: 10.1021/acs.jpcb.7b09700 • Publication Date (Web): 14 Nov 2017

Effect of Substrate Temperature on Pattern Formation of Bi-Dispersed Particles from Volatile Drops

Maryam Parsa, [1,2] *Souad Harmand,* [*,1,2] *Khellil Sefiane,* [3,4] *Maxence Bigerelle,* [1,2] *and Raphaël Deltombe* [1,2]

[1]LAMIH Laboratory, UMR CNRS 8201, University of Valenciennes, Valenciennes 59313, France

[2]University of Lille Nord de France, Rue Jules Guesde, Villeneuve d'Ascq 59658, France

[3]School of Engineering, Kings Buildings, University of Edinburgh, Edinburgh EH9 3JL, United Kingdom

[4]International Institute for Carbon-Neutral Energy Research (I2CNER)

Kyushu University, 744 Motooka, Fukuoka 819-0395, Japan

ABSTRACT

In this study, pattern formation during evaporation of bi-dispersed drops (containing 1 and 3.2 μm particles) placed on a smooth substrate at different temperatures is investigated. Five distinctive deposition patterns are observed depending on the substrate temperature: a relatively uniform pattern enclosed by a disk-shaped ring, a nearly non-uniform pattern inside a thick outer ring, a "dual-ring" pattern, a "rose-like" pattern, and a set of concentric rings corresponding to "stick-slip" pattern. At drops edge, the particle size effect leads to the formation of three rings: an outermost ring formed by the non-volatile additives smaller than 1 μm, a middle ring built by particles with size of 1 μm, and an innermost ring formed by the mixture of 1 and 3.2 μm. For temperatures between 64 and 99 °C, the depinning of the contact line causes the same particle sorting at the other deposition lines in the interior of the drop. However, the width of the zone between the outermost ring and the middle ring at the initial edge of the drop is found to be smaller than that at the other deposition lines. The size of the width is found to be dependent on the contact angle. Particle velocity is measured by tracking particles during the evaporation. It is shown that particle velocity slightly increases with time, but it rapidly increases at the last stage of the drying process, known as "rush-hour" behavior. The sudden change in the increase of the velocity occurs between the normalized time of 0.7 and 0.8 for temperatures from 22 to 81 °C. The increasing trend of velocity with time matches well with the theoretical model. The tracer particles are also used to measure the distance between the contact line and the nearest turning point of those particles return back toward the top of the drop due to the inward Marangoni flow. It is found that this distance decreases with increasing the substrate temperature.

INTRODUCTION

The drying of a sessile droplet containing nonvolatile solute can lead to the formation of a deposition pattern on the substrate. A full understanding of the pattern formation is of vital importance as it plays a crucial role in many industrial applications such as inkjet printing,[1–4] lithography,[5] micro-patterning of electronics,[6] and photonics.[7] Moreover, the study of the pattern formation is of increasing biological importance.[8,9] The most commonly observed pattern is the "coffee-ring" effect or the ringlike deposit, which is created by the deposition of particles at the edge arisen from the net outward capillary flow on the liquid-solid interface.[10,11] It is well known that the "coffee-ring" effect can be reversed by the inward Marangoni flow driven by the surface tension gradient along the liquid-vapor interface.[12] The inward Marangoni flow causes some particles travel toward the center along the free surface, and deposit in the central regions of the drying droplet. This phenomena leads to the formation of different patterns such as the uniform deposition, "dual-ring",[13] "stick-slip",[13] and volcano-like patterns.[14] There are a number of factors affecting the pattern formation, which can be manipulated to control internal flow motion as well as the dried deposits for use in the aforementioned applications such as altering environmental conditions (i.e. atmospheric pressure,[15] substrate temperature,[13,14] relative humidity[16]), applying electrowetting,[17,18] manipulating the base fluid,[19,20] adding surfactants,[21–23] varying the solute (i.e. shape,[24] size, concentration[25,26]).

Another factor that affects the deposition patterns is to employ different particle sizes inside a drying droplet simultaneously. Huang et al.[27] showed that the mixture of 50 nm silver and 100 nm gold nanoparticles in water forms well-aligned stripe patterns onto a silicon-dioxide/silicon substrate through dip-coating. Jung and Kwak[28] reported that 1 and 6 μm polystyrene particles can be separated using the dielectrophoretic (DEP) force created by the micropatterned gold

electrode on the silicon dioxide layer and the drag force generated by the outward flow in an evaporating droplet. The authors showed that the two sized particles self-assembled near the contact line. The smaller particles deposited at the edge, whereas the larger ones deposited separately with a constant distance (of ~ 67 μm) from the smaller ones. The separation of the red blood cells (RBCs) and Escherichia coli (E. coli) was also observed by the same method.[28] Erb et al.[29] applied the magnetostatic interaction between 1 and 2.7 μm Fe_2O_3 particles to assemble diverse sets of structures such as rings (a large particle is surrounded by smaller particles), and poles (small particles aggregate on two sides of a large particle). Jung et al.[30] divided the dispersing of the polystyrene micro- (5 μm) and nanoparticles (500 nm) in an evaporating droplet into the three phases by using particle-tracking velocimetry (PTV). In the first phase, the micro- and nanoparticles migrated toward the pinned contact line and deposited there. In the second phase, the separation of the two sized particles near the contact line was observed similar to Jung and Kwak.[28] In the third phase, the receding contact line causes the movement of the microparticles toward the center of the droplet. Sangani et al.[31] also reported that the small particles (of 3 μm) moved toward the contact line and deposited at the drop edge, leading to the contact line pinning. On the other hand, the larger particles (of 50 μm) collected as a chain with keeping a distance from the small ones. The distance between the chain of the large particles and the edge increases slowly with time as the drop height decreases, and thus, the chain moves inward. However, unlike the bi-disperse suspension, this distance between the particles and the edge remained nearly constant in most monodisperse suspension cases.[31] Weon and Je[32] also observed the increasing distance between the chain of large polystyrene particles (20 μm) and the drop edge, while small particles (2 μm) segregated at the edge. The authors concluded that the reversal motion of large particles happens when the inward force driven by the capillary force

overcomes the outward force driven by the "coffee-ring" effect. This competition between these two forces affected the pattern left after the evaporation of 0.2 and 3.6 μm diameter polymethylmethacrylate (PMMA) particles in water.[32] At first, the initial ring of small particles at the edge was formed, and then, the large particles moved inwardly to the central regions, then a new ring of deposits was formed when the reverse motion was stopped by rupture. This behavior was repeated for several times and consequently multiple rings were formed on the substrate.[32] Chhasatia and Sun[33] studied the evaporation of bi-disperse drop containing 0.1 and 1.1 μm particles on substrates with different wettabilities (receding contact angle varied from 85° to 0°). Since the state of substrate wettability significantly affects the duration of evaporation modes (i.e. constant contact area, constant contact angle, and mixed modes), different microflow patterns within evaporating drops were observed for each evaporation mode. As a result, different deposition patterns were found for substrates of varying wettabilities.[33] Monteux and Lequeux[34] showed a thin liquid film without particle at the edge in the case of monodisperse drop. The width of the depleted zone was found to be controlled by the particle size and contact angle. This phenomenon was reported to be useful to sort two different particle sizes inside the drop as the smaller particles can penetrate further into the edge, leading to the separation of smaller particles from the larger ones. Wong et al.[35] studied the deposition of three different sized polystyrene particles (of 40 nm, 1, and 2 μm) in a water droplet. The largest and smallest particles formed the innermost and outermost rings on the substrate after the dryout of the droplet, respectively. Devlin et al.[36] investigated the effect of the gravity direction on the deposition patterns of two different (1 and 3.2 μm) sized particles in a sessile and a pendant drop both deposited onto silicon substrates. For the pendant drop, only small particles deposited at the edge, and the dried central region contained the large particles. However, for the sessile drop, the

mixture of 1 and 3.2 μm sized particles deposited at the edge,[36,37] and both two particle sizes were found in the center of the dried drop.[36] Zhong et al.[38] reported that the evaporation of water sessile droplets with 40 nm Al_2O_3 nanoparticles left behind a fractal-like deposit, whereas the 5 nm nanoparticles formed a coffee-ring pattern with a thick deposition in the center of the dried droplet. The authors demonstrated that the coexisting of 5 and 40 nm Al_2O_3 nanoparticles eliminated the nonuniform pattern formed either by the 5 or 40 nm nanoparticles, leading to a more uniform mixture pattern.

A review of the relevant literature indicates that most studies have been devoted to understanding the behavior of multi-sized particles in liquid drops evaporating on nonheated substrates.[27–38] However, there are only a few works have investigated the influence of heated substrates in this field.[39–41] Han et al.[39] showed that two different particle sizes of 50 and 500 nm can self-assemble into arranged stripe patterns by confining the solution between a cylindrical lens and heated hydrophobic silicon substrate at 80 °C. Jeong et al.[40] showed that a combination of the "coffee-ring" and strong Marangoni effects can be used to sort different sized particles (from 100 nm to 15 μm) on a hydrophilic substrate heated at 36 °C. The particles were not separated on hydrophobic substrates due to the constant, large contact angle as well as the unpinned contact line during the evaporation, leading to the transportation of the particles away from the contact line. Eventually, the particles of different sizes were overlapped at the contact line on hydrophobic surfaces. Hendarto and Gianchandani[41] investigated the effect of Marangoni convection on the size sorting of multiple-sized hollow glass spheres (ranging from 5 to 200 μm in diameter) suspended in a isopropyl droplet by heating a glass substrate for a wide range of temperatures (55 to 85 °C). Although the smaller spheres (< 50 μm) were found everywhere throughout the dried droplet at 55 °C, the larger spheres (150-200 μm) were mainly deposited in

the center of the dried region. At 85 °C (over the boiling point of isopropyl), most of the smaller spheres were deposited at the areas near the edge.

To the best of our knowledge, there is no article available to study the effect of various temperatures on the mixture of two sized particles suspended in water-based sessile droplets. However, in recent years, very interesting studies related to the effect of substrate temperature on the deposition patterns of a single sized particles suspended in water-based droplets are published. As an example, Parsa et al.[13] found that varying temperature led to the formation of three deposition patterns: a "uniform" pattern, a "dual-ring" pattern, and a "stick-slip" pattern. Li et al.[42] and Patil et al.[43] reported that increasing the substrate temperature left an inner deposit in the interior of the dried droplet. Zhong and Duan[44] observed that cooling to heating of the substrate varied the deposition patterns from a "disk-like" pattern to a "dual-ring" one. The authors also showed that the further increase of the substrate temperature expanded the inner ring and merged it with the peripheral ring, leading to the elimination of the "dual-ring" pattern.[45]

In this study, the effect of a wide range of substrate temperatures (from 22 to 99 °C) is investigated on the internal flow structure as well as the deposits features of two different sized particles in water droplets drying on smooth silicon substrates. In addition, for the first time, the motion of two sized particles is tracked within a drying droplet on a heated substrate using reflection optical microscopy.

EXPERIMENTAL PROCEDURE

Solution. The aqueous suspension was made from yellow-green fluorescent carboxylate-modified polystyrene latex beads with mean diameter of 1 μm (Sigma-Aldrich), and Fluoro-Max^{TM} red fluorescent polymer microspheres with diameter of 3.2 μm (Thermo Scientific) in MilliQ water. Then, the suspension was thoroughly mixed and sonicated in an ultrasonication

bath for approximately 1 h prior to the experiments to ensure appropriate mixing. The mass concentration of particles was 0.025 wt % with equal parts of each particle size.

Deposition. Smooth silicon wafers were ultrasonicated and thoroughly rinsed with deionized water and acetone, followed by air drying (Elma Company) to remove the moisture. A programmable syringe pump (KdScientific, legato 100) was used to deposit the drop solution (with varying size from 0.5 to 6 μL) onto the hot silicon substrate which was placed on a plate heated at temperatures of 51, 64, 81, and 99 °C. The experiment was also carried out onto nonheated substrate (22 °C). Each set of experiment was repeated for at least five times. The atmospheric conditions were monitored during the experiments using a sensor (Hygrosens Company). The room temperature and relative humidity were 22 °C and 30%, respectively.

Imaging and Microscopy. Thermal imaging was conducted by means of an infrared (IR) camera (FLIR, X6580 sc) mounted on a lens (FLIR, MW G1WD30) to read the temperature at the air-liquid interface of the drying droplets, as water is mostly opaque to IR (see Figure S1 in Supporting Information). A high-speed camera (Keyence, VW600C) equipped with a lens (Keyence, VW Z2) and a LED backlight (CCS Inc.) were employed to record side view images of evaporating droplets at 30 frames per second. The drop shape analysis software (Krüss GmbH, DSA4) was used to monitor the evolution of drop shape parameters such as the base diameter and contact angle. The top view images of evaporating droplets were recorded by means of the high-speed camera mounted on an optical microscopic lens (Keyence, VH-Z100R, magnification zoom from 100× to 1000×). The particles movement was tracked using video editing/analysis software (Keyence, VW-9000 Motion Analyzer). The images of the final deposition patterns were taken by using an optical microscopic lens (Keyence, VH-Z20R, magnification zoom from 20× to 200×). In order to investigate the deposition distribution along the droplet base diameter,

the dried deposits were scanned by means of a white light interferometer (Zygo, NewView 7300). The further information about characterization and quantification of substrate roughness can be found in the study of Parsa et al.[13] The uncertainties of the measurements are provided in Table 1.

Parameters	Uncertainty
Ambient temperature	± 0.5 °C
Relative Humidity	± 2 %
Surface temperature of drop	± 1 °C
Particle velocity	± 2 μm/s
Base of drop	± 0.4 mm
Contact angle	± 4°
Initial volume	± 2.5 μL

Table 1. Experimental uncertainties.

RESULTS AND DISCUSSION

Deposition Pattern after Dry-out of Drops. Figure 1a shows the contact line of drops remain pinned for majority of the evaporation time, and the contact angle monotonously decreases. Dried Patterns of bi-disperse drops at different temperatures from 22 to 99 °C are presented in Figure 1b. Using an algorithm, the 3.2 μm particles are separated from the 1 μm particles, and the density corresponding images are provided in Supporting Information. Dried deposits of drops, density distribution and topography of the particle deposits are shown in Figures S2, S3, and S4, respectively.

As shown in Figures 1b, S3 and S4, sample I at 22 °C exhibits a relatively uniform coverage of particles enclosed with a distinct disk-shaped ring of particles. For sample II at 51 °C, the observed pattern shows nearly non-uniform distribution of particles inside the outer ring with a

higher density. As shown in Figures 1b and S3-4, samples at temperatures of 64, 81, and 99 °C exhibit completely non-uniform patterns compared to the examined lower temperatures. At 64 and 81 °C, the "dual-ring" pattern is observed with the irregular distribution of particles in the interior of the smaller ring (see Figures 1bIII,IV, S3III,IV and S4III,IV). At 99 °C, both samples V and VI exhibit the "stick-slip" patterns but in two different shapes; one resembles a "rose" flower wherein both the "stick" and "slip" phases occur on all sides of the drop, and end in the drop center (Figures 1bV, S3V and S4V); and the other resembles a set of multiple concentric rings wherein the drop sticks on one side (the left side of Figures 1bVI, S3VI and S4VI) and slips from the opposite side (the right side of Figures 1bVI, S3VI and S4VI). The density of particles increases at the deposition lines and decreases between two consecutive lines (see Figures S3V,VI and S4V,VI).

Deposition Formation during Drying Process. Using optical microscopy, the evaporation process of bi-disperse drops at all substrate temperatures was observed (see Supporting Information). The readers are strongly encouraged to view the high magnification videos provided in the Supporting Information, as the motion of particles cannot be unambiguously ascertained from still images. Top-view snapshots from all real-time videos of the drying bi-disperse drops are provided in Figures 2,3,6,7,10-15. In all figures, the microscope lens was focused on the contact line of drops. The 1000× magnification consecutive optical micrographs of the drop evaporating on the nonheated substrate are shown in Figure 2 (Supporting Information Video S1). Insets in Figure 2 show the regions highlighted in solid rectangles at higher magnification. It can be clearly seen that the accumulation of particles at the edge increases with time due to an outward radial flow driven by the "coffee-ring" effect (see Figure 2a-i). It is known that the thickness of the meniscus decreases toward the drop edge, thus

particles stop moving further toward the contact line at a position where their size match the thickness of the meniscus.[35] In other words, the smaller particles move closer to the pinned contact line as compared to the larger ones, leading to the separation of particles with different sizes (insets in Figures 2b,e,h). Magnified images of the CL region show that there is a thin liquid film between the initial contact line and leading edge of the ring consisting of particles with mean diameter of 1 μm (shown between two arrows in inset in Figure 2e). A peripheral ring of particles is left behind at the drop edge after the complete evaporation confirming that the thin liquid film did not only consist of pure water (see the outermost ring in inset in Figure 2i). Besides, Figure 3 shows a depleted zone is left behind between the peripheral ring and the leading edge of 1 μm particles after the complete evaporation of the thin liquid film separating the two rings from each other. In order to ensure the origin of the deposits at the peripheral ring, the evaporation of drops containing monodisperse particles was conducted (Figure 4). As presented in Figure 4aI, the drop containing 1 μm particles leaves a thin liquid film which is between the particles and the contact line. After the complete evaporation, only a single ring at the periphery is left, and thus the thin liquid film of pure water is completely evaporated (see Figure 4aII). Figure 4bI shows the 3.2 μm particles travel toward the edge and stop from the edge with a distance, which is filled with the thin liquid film. As shown in Figure 4bII, two rings of particles are left behind after the drop dries out. The inner ring is formed by 3.2 μm microspheres; the outer (or peripheral) ring is formed by the particles obviously smaller than 3.2 μm microspheres (Figure 4bII). This results from the deposition of the non-volatile additives, which are used in the monodisperse 3.2 μm particles suspension by the manufacturer to inhibit agglomeration and promote stability of the suspension. The same peripheral ring can be seen for dried bi-disperse drops. This reveals that the smallest particles probably with diameters lower

than 1 μm penetrate further inside the contact line region, and reach the drop edge, leading to the deposition of particles there. Therefore, three separate rings of particles can be observed during the drying process of bi-disperse drops (see insets in Figure 2h): the first is the outermost ring at the contact line consisting of particles smaller than 1 μm; the second is the middle ring forming by 1 μm particles; and the third is the innermost ring consisting of 3.2 μm particles. To better understanding of the deposition features in the vicinity of the contact line, the individual particles within the droplet were tracked, as shown by the blue and red arrows in Figures 5aI-5aVI. The arrows show that those 1 μm particles arriving behind the 3.2 μm particles can travel around the larger particles and reach the middle ring. Besides, some 1 μm particles pass from between the two adjacent 3.2 μm particles and then deposit at the middle ring (shown by the circle in Figures 5bI-5bIV). Such movements by small particles can be observed until the late stages of the evaporation. On the other hand, some other small (1 μm) particles are trapped at the innermost ring, and cannot move further toward the edge due to the presence of high number of large particles at the innermost ring at the late stages of the evaporation (see the increase in the number of particles of the innermost ring with time in Figure 2a-h). In addition, there is a dramatic increase in the velocity of particles approaching the edge in the late stages of the drop's lifetime,[46,47] causing the sudden increase in the number of small particles at the innermost ring. In other words, there is no enough space for these small particles to pass through the inner ring, and reach the middle one, leading to the aggregation of small particles at the innermost ring, and hence the innermost ring is formed by the mixture of both small (1 μm) and large (3.2 μm) particles after the dry-out of the drop (see the innermost ring in insets in Figure 2i). Insets in Figure 2b,e,h show that the distance between the innermost ring and the contact line increases with the evaporation time. In other words, the innermost ring moves inward toward the drop

center, repelling the "coffee-ring" effect. The reversal motion of the innermost ring can be attributed to the inward force driven by the capillary force,[48,49] which is found to be a kind of lateral immersion capillary force.[48] The latter acts when there is a contact between the particles and the air-liquid interface during the drying process.[48,49] The inward migration of particles takes place whenever the outward coffee-ring flow is overcome by the net capillary force between particles and the air-liquid interface, which is consistent with literature.[32] This reverse effect is a unique transport mechanism which is related to the geometric constraints of particles and drop (i.e. drop size, contact angle),[32] instead of other mechanisms such as the Marangoni,[12,50] gravity and standard effects,[10,11] etc.

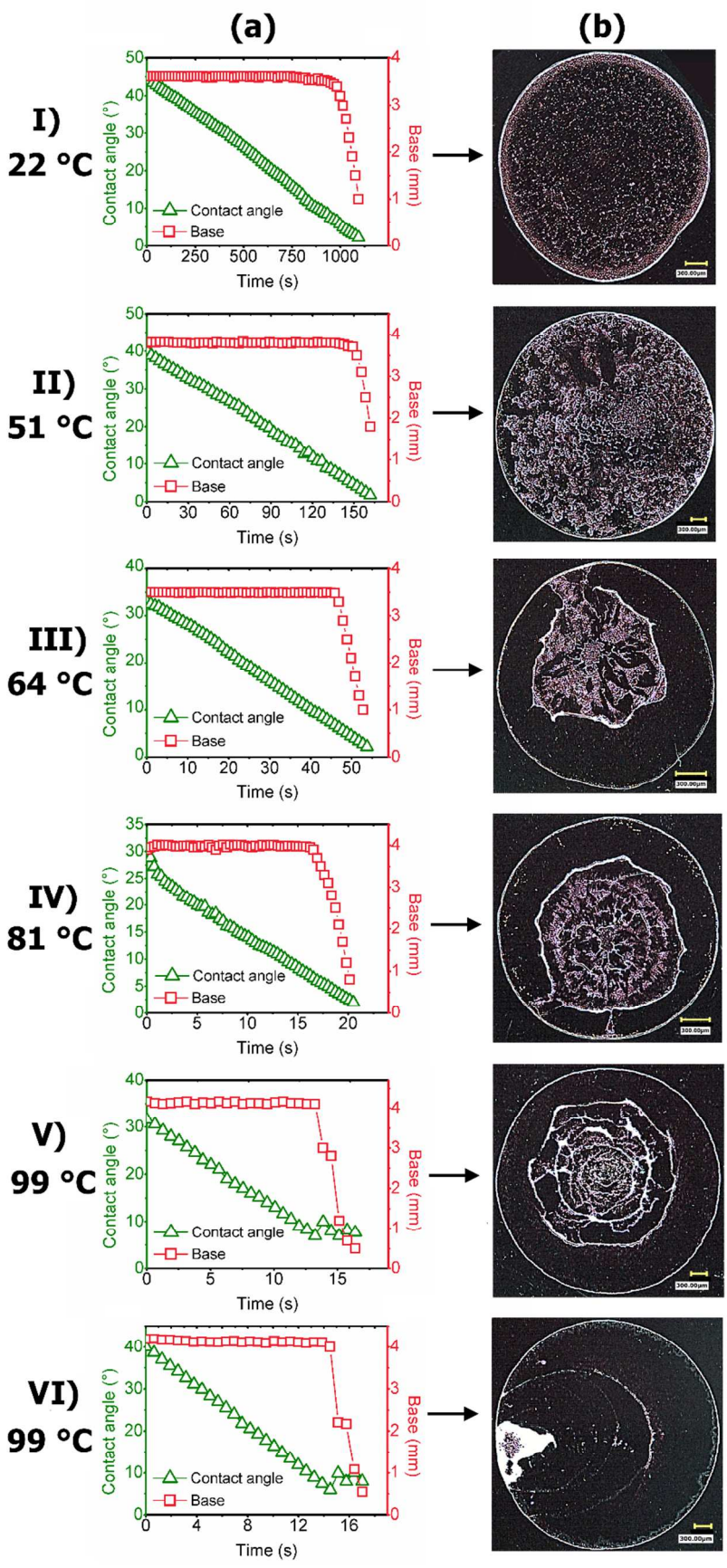
(a)
(b)
I)
22 °C
II)
51 °C
III)
64 °C
IV)
81 °C
V)
99 °C
VI)
99 °C
Contact angle (°)
Base (mm)
Time (s)
Contact angle
Base

Figure 1. (a) Evolution of base and contact angle for evaporating water-based bi-disperse drops containing a mixture of 3.2 μm diameter particles (mass concentration of 0.0125 wt %) and 1 μm mean diameter particles (mass concentration of 0.0125 wt %) onto a nonheated silicon substrate (at 22 °C) and heated substrates at different temperatures of 51, 64, 81, and 99 °C. The initial volume of drops at different temperatures: (aI) 4, (aII) 4.1, (aIII) 2.6, (aIV) 3.2, (aV) 4.1, and (aVI) 5 μL. (b) Dried deposits of bi-disperse drops onto a nonheated silicon substrate (at 22 °C) and heated substrates at different temperatures of 51, 64, 81, and 99 °C. Scale bars, 300 μm.

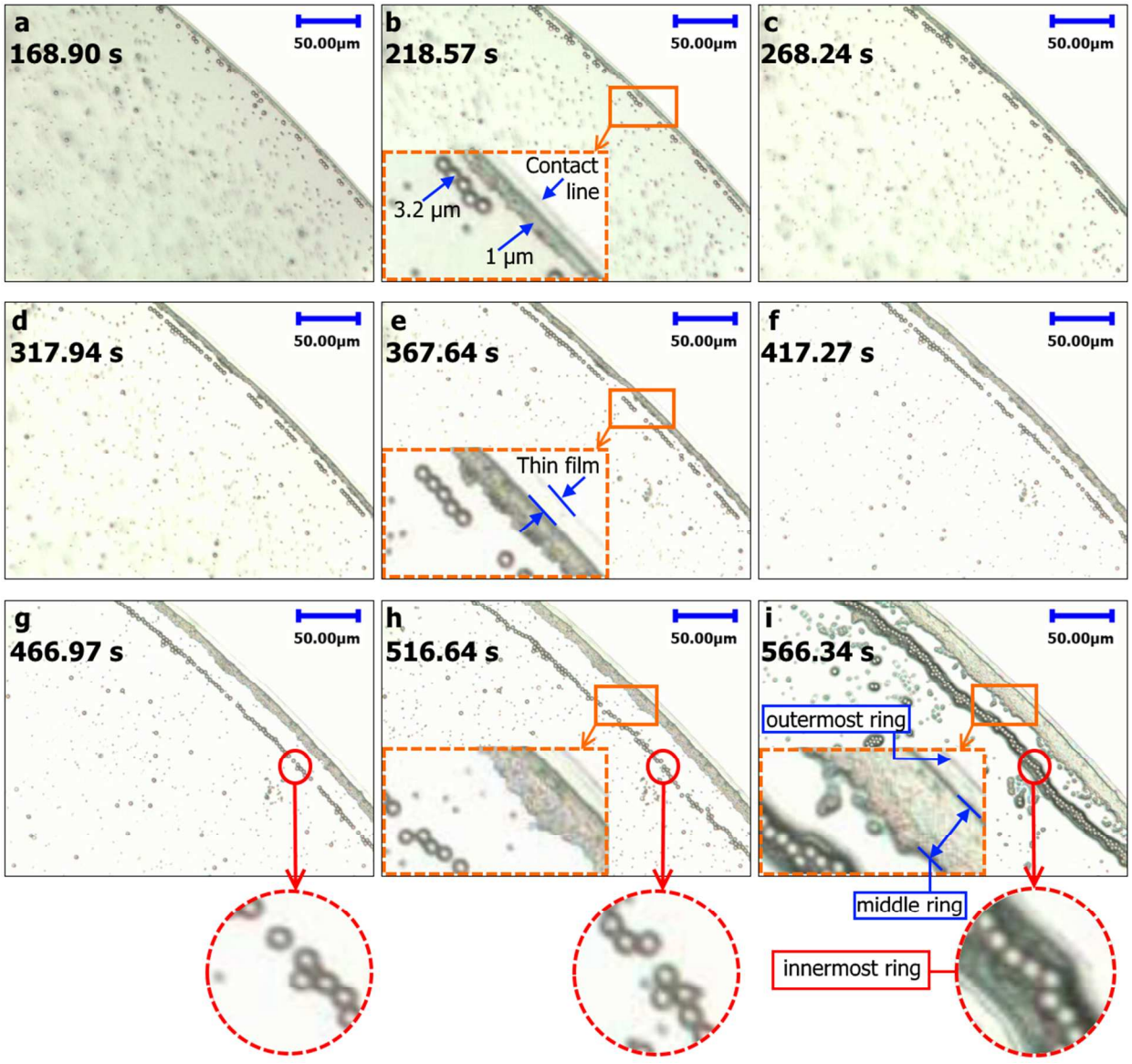

Figure 2. Snapshots from a video microscopy of the evaporation process of a 3 μL water-based bi-disperse drop containing a mixture of 3.2 μm diameter particles (mass concentration of 0.0125 wt %) and 1 μm mean diameter particles (mass concentration of 0.0125 wt %) onto a nonheated silicon substrate (at 22 °C). Insets show the zoomed in regions highlighted in the solid rectangles and circles. The micrographs are recorded at a temporal resolution of 30 fps and at 1000× magnification. Scale bars, 50 μm.

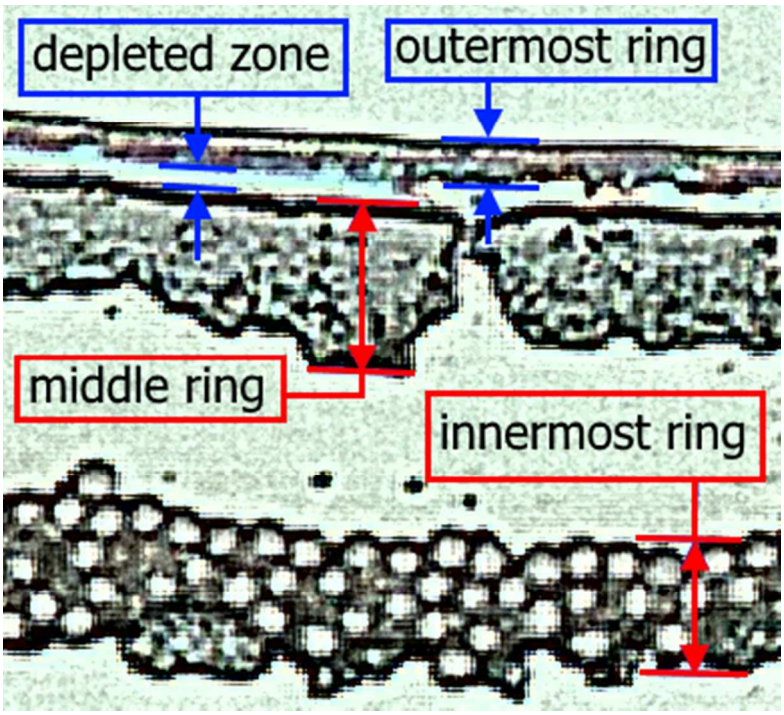

Figure 3. 2× zoomed in picture of a completely dried 3 μL water-based bi-disperse drop containing a mixture of 3.2 μm diameter particles (mass concentration of 0.0125 wt %) and 1 μm mean diameter particles (mass concentration of 0.0125 wt %) onto a nonheated silicon substrate (at 22 °C). The complete evaporation of the thin liquid film leaves a depleted zone between the leading edge of the middle and outermost rings. The original micrograph is taken at magnification of 1000×.

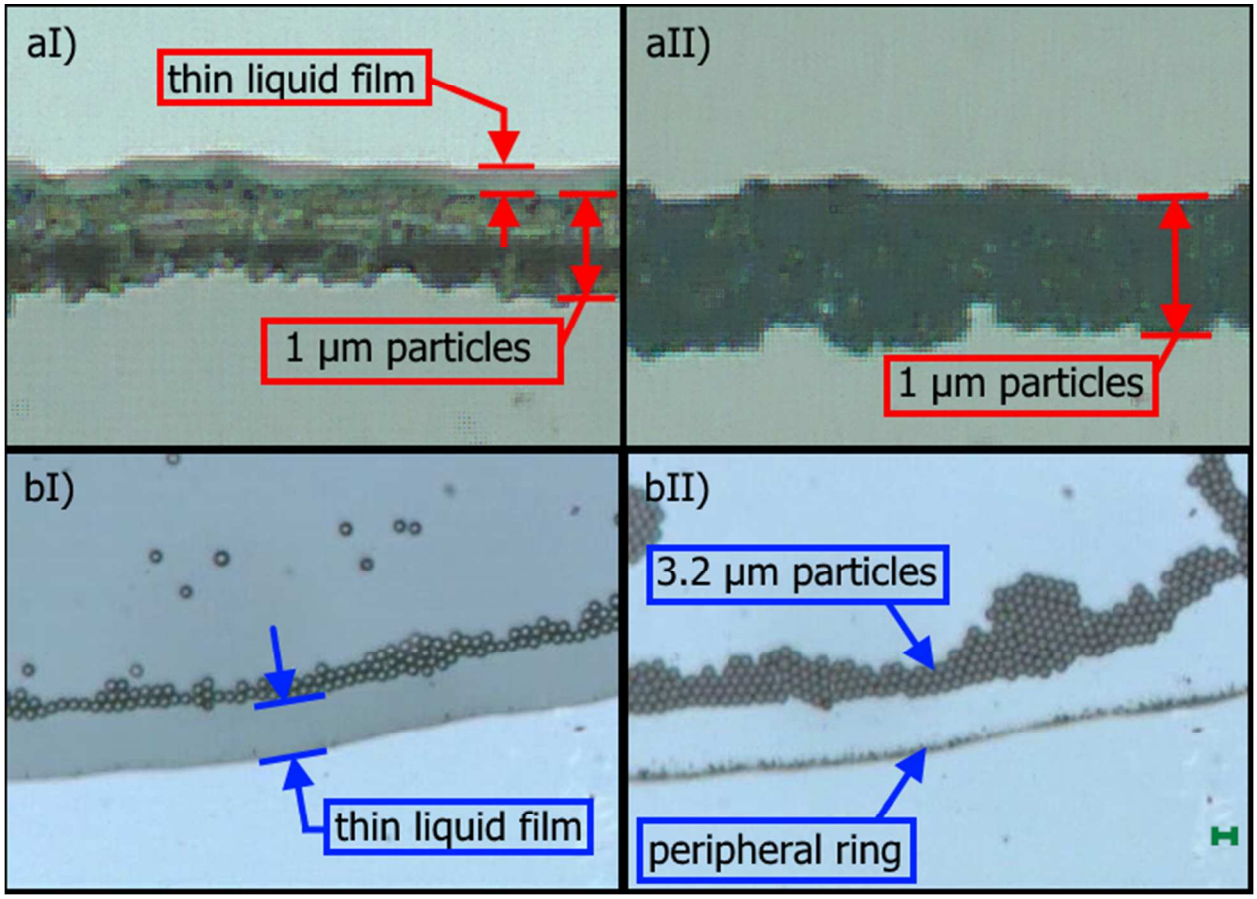

Figure 4. (a) Images taken from a video microscopy of the evaporation process of a 3 μL water-based monodisperse drop containing 1 μm mean diameter particles (mass concentration of 0.0125 wt %) onto a heated silicon substrate at 51 °C: (I) The 1 μm particles leave a thin liquid film during the evaporation; (II) The thin liquid film dries out at the end of the evaporation, and only the ring of 1 μm particles is left behind. (b) Images taken from a video microscopy of the evaporation process of a 3 μL water-based monodisperse drop containing 3.2 μm diameter particles (mass concentration of 0.0125 wt %) onto a heated silicon substrate at 51 °C: (I) The thin liquid film is formed between the edge and the ring of 3.2 μm particles during the drying; (II) The thin liquid film dries out at the end of the evaporation and leaves the peripheral ring of non-volatile additives behind, apart from the inner ring of 3.2 μm particles. Scale bar, 6 μm.

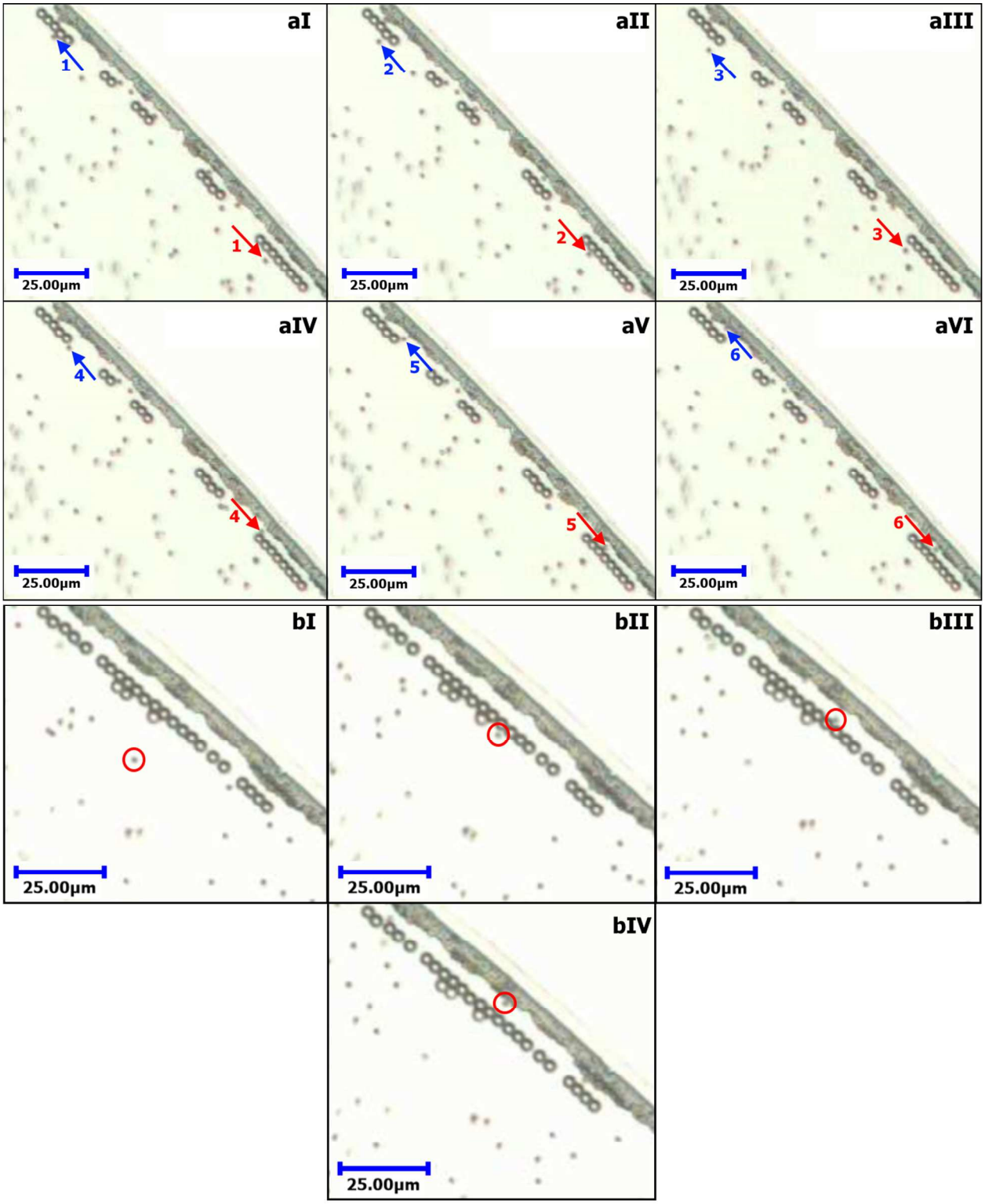

Figure 5. Zoomed in snapshots from a video microscopy of the evaporation process of a 3 μL water-based bi-dispersed drop containing a mixture of 3.2 μm diameter particles (mass

concentration of 0.0125 wt %) and 1 μm mean diameter particles (mass concentration of 0.0125 wt %) onto a nonheated silicon substrate (at 22 °C). (aI-VI) The two-color arrows indicate two tracers 1 μm particles which move toward the edge; the particles become close to the 3.2 μm particles, and then travel around them and deposit at the middle ring near the edge. (bI-IV) The circle indicates a tracer 1 μm particle which moves toward the edge; the particle passes from between the two adjacent 3.2 particles and deposit at the middle ring. The micrographs are recorded at a temporal resolution of 30 fps and at 1000× magnification. Scale bars, 25 μm.

The 1000× and 100× magnification consecutive micrographs of the evaporating droplets on the substrates heated at 51 °C are given in Figures 6 and 7, respectively (Supporting Information Videos S2 and S3). A thin liquid film can be seen between the contact line and leading edge of the middle ring (formed by 1 μm particles) similar to what observed for the nonheated case (see inset in Figure 6g). The 3.2 μm particles also deposit in the vicinity of the middle ring and forming the innermost ring but it is not well-organized as that observed at 22 °C (see insets in Figure 6g,h). Unlike the nonheated case, the reverse effect (observed for the nonheated case) is not seen at 51 °C, and thus the innermost ring is not transported inwardly toward the center. Instead, the Marangoni effect plays an important role in the transportation of particles in the reverse direction of the outward flow. The tracking of particles reveals that in the early stages of the evaporation, a group of particles approach the drop edge but do not reach the edge. Instead, they move back radially toward the top of the drop surface along the air-liquid interface. These repelled particles stop near the top of the drop surface, building a ringlike collection (or cluster) of particles there (see Figure 7a-e). The transportation of particles toward and away from the drop edge forms an eddy region between the ringlike cluster at the top region of the drop and the edge, as shown by the double arrows between the dashed curve and edge in Figure 6a-h. It is

well understood that there is a surface tension gradient along the air-liquid interface as the temperature on the top center of the drop is lower than the edge.[13,51] The surface tension of water decreases with increasing temperature, and water tends to flow to high surface tension regions; thus, the radially inward flow is driven from the edge to the top surface of the drop. Moreover, the existence of a stagnation point at the air-liquid interface near the contact line divides the internal flow inside the evaporating drop into two regions (see Figure 8):[50] one is an outward surface flow which is beyond the stagnation point, leading to the motion of particles toward the contact line close to the solid surface and their deposition at the edge; the other is the convective flow, in which particles move radially outward toward the drop edge but then their direction is changed and move backward along the air-liquid interface (Figure 8). It is reported that in the case of having both the strong Marangoni effect and stagnation point, only those particles participating in the outward flow region can deposit in the edge regions,[52] and build the three rings structures. Therefore, those particles participating in the convective flow region lead to the formation of the ringlike cluster of particles at the top surface of the drop. During the late stages of the evaporation (just before the depinning of the contact line), the ringlike cluster moves toward the contact line (Figure 7f), and a group of particles deposit near both the middle and innermost rings, merging these two rings completely (see inset in Figure 6i). On the other hand, as both the arrival of the ringlike cluster toward the edge and depinning are two immediate, consecutive processes, a group of particles at the free interface of the drop may not have the time required to reach the edge, and thus freezes in place, forming a non-uniform distribution of particles inside the drop (Figure 7f-i). In the merging process of the two inner rings, the majority of smaller particles (1 μm) deposit closer to the edge compared to the larger ones (3.2 μm). This is because of further penetration of the small particles into the regions near the contact line in

comparison with the larger ones. The contact line depinning occurs just after the merging of the middle and innermost rings, preventing the deposition of the ringlike cluster as a new ringlike structure in the central regions of the drop. Side views of an evaporating droplet deposited onto a heated substrate is sketched based on the aforementioned analysis. In Figure 9a,b, the solid and dashed arrows indicate the direction of the outward and thermal Marangoni flows, respectively. First, the outward flow causes the particles to move adjacent to the substrate surface toward the initial contact line and deposit near the edge (Figure 9a,b). However, the Marangoni flow prevents a fraction of these particles from depositing at the edge and leads them to return inwardly along the air-liquid interface (Figure 9a,b). The collection of these particles at the top surface of the drop results in a ringlike cluster. The cluster approaches the drop edge before the depinning of the contact line (Figure 9cI), joining the particles deposited near the edge (Figure 9dI). The depinning occurs quickly after the merging (Figure 9dI), hence the ringlike cluster does not deposit as a distinct ringlike structure in the central regions of the droplet, unlike the other studies.[13,44,51,53] Several works[13,42,43,45] reported the similar ringlike cluster at the top of evaporating nanofluid droplets (Figure 9a,b), which deposited as a distinctive secondary ring or an inner deposit in the central regions of the dried droplet. Parsa et al.[13] observed that first the contact line depinned (Figure 9cII), and then the cluster drifted toward the depinned contact line (Figure 9dII).[13] Consequently, a new ringlike structure was formed when the ringlike cluster reached the depinned contact line (Figure 9dII,eII).[13] By comparing the present observations (Figure 9cI,dI,eI) with those of Parsa et al.[13] (Figure 9cII,dII,eII), it can be concluded that the depinning time of the contact line plays an important role in the final deposition pattern. The previously observed thin liquid film between the contact line and leading edge of the middle ring dries out only at the last moments of the evaporation process (insets in Figure 6g,h,i). After the

complete evaporation, a new peripheral ring appears at the drop edge which is separated from the merged ring by a depleted zone (see inset in Figure 6i). The similar ring was also observed for the nonheated case, (marked as the outermost ring in Figure 6i).

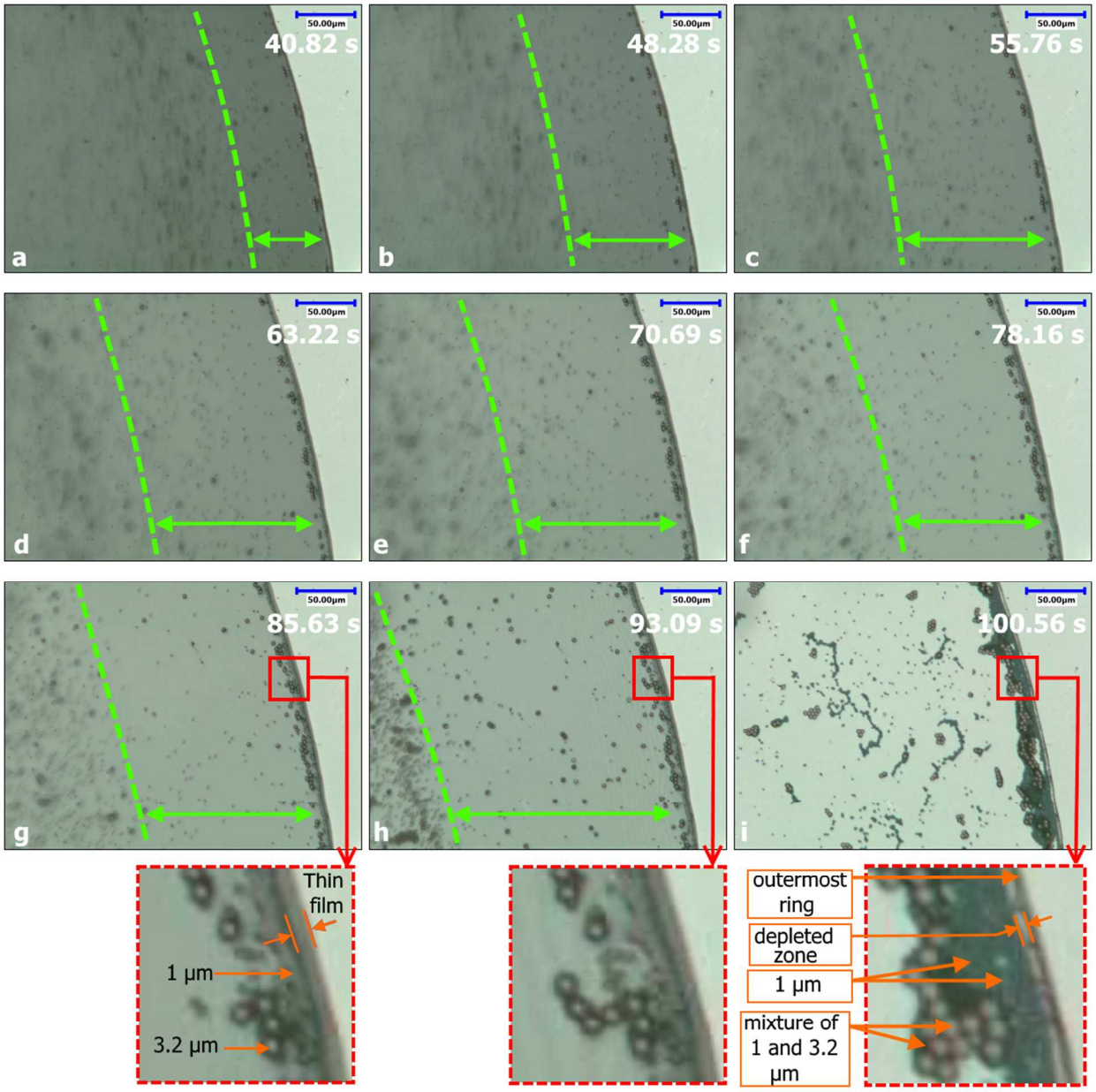

Figure 6. Snapshots from a video microscopy of the evaporation process of a 3 μL water-based bi-disperse drop containing a mixture of 3.2 μm diameter particles (mass concentration of 0.0125 wt %) and 1 μm mean diameter particles (mass concentration of 0.0125 wt %) onto a heated

silicon substrate at 51 °C. The double arrows denote the eddy region between the ringlike cluster and edge. Insets show the zoomed in regions highlighted in the solid rectangles. The micrographs are recorded at a temporal resolution of 125 fps and at 1000× magnification. Scale bars, 50 μm.

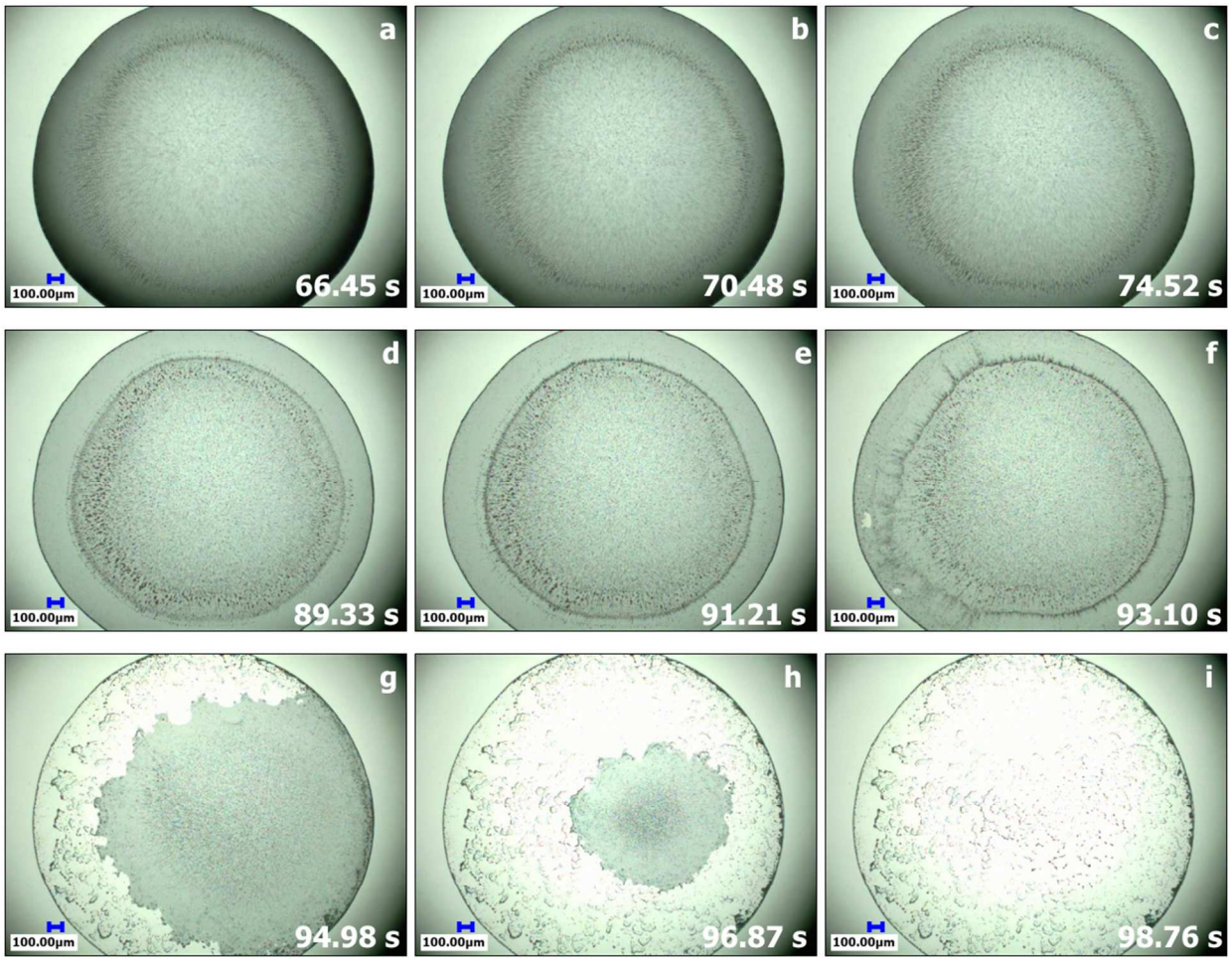

Figure 7. Snapshots from a video microscopy of the evaporation process of a 3 μL water-based bi-disperse drop containing a mixture of 3.2 μm diameter particles (mass concentration of 0.0125 wt %) and 1 μm mean diameter particles (mass concentration of 0.0125 wt %) onto a heated silicon substrate at 51 °C. The micrographs are recorded at a temporal resolution of 125 fps and at 100× magnification. Scale bars, 100 μm.

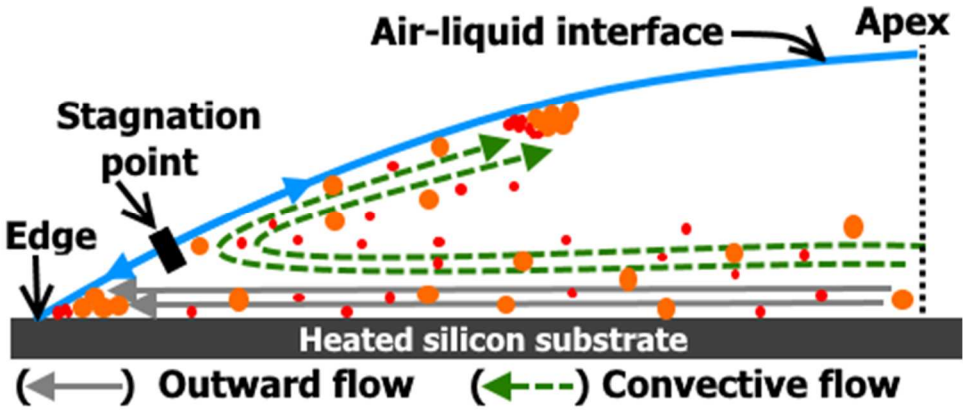

Figure 8. Sketch of the internal flow pattern inside an evaporating water-based bi-disperse drop containing a mixture of 3.2 μm diameter particles and 1 μm mean diameter particles onto a heated silicon substrate; The outward and temperature-dependent Marangoni flows are indicated by the solid and dashed arrows, respectively. The black bar indicates a stagnation point where the surface flow changes its direction.

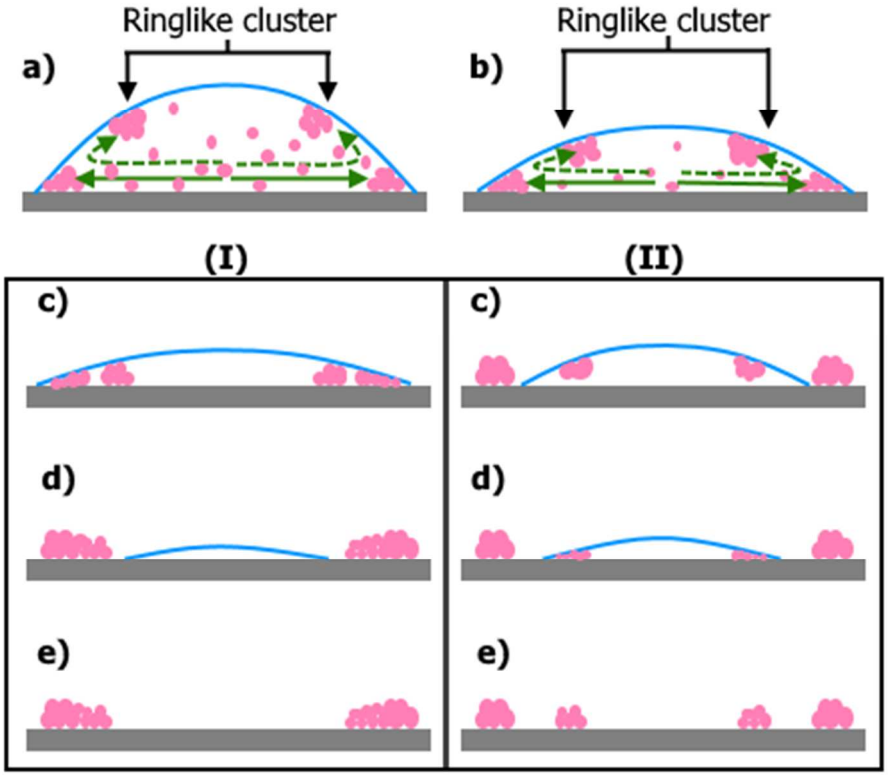

Figure 9. Deposition mechanism schematic of the ringlike cluster onto the heated silicon substrate during and after the evaporation of a water-based drop containing particles: (a) The particles move toward the pinned edge (shown by the solid arrow), some deposit at the edge, and a fraction of the particles move back inward to the top surface of the drop. (b) The number of particles increases with evaporation time at the top surface and edge, leading to the formation of a ringlike cluster at the top region of the droplet near the air-liquid interface. (cI) The ringlike cluster move toward the pinned edge, and join particles deposited at the edge. (dI) The contact line depins. (eI) After the complete evaporation, the ringlike cluster deposited in the edge regions, merged with the other particles at edge. (cII) The contact line depins, and the ringlike cluster move toward the depinned contact line. (dII) The ringlike cluster reach the depinned contact line and deposit in the central region. (eII) Apart from the particles deposited in the edge regions, the deposition of the ringlike cluster leads to a new distinct ringlike structure in the central regions after the complete dry-out of the drop.

The 1000× and 100× magnification consecutive still images of the evaporating drop at 64 °C are provided in Figures 10 and 11, respectively (Supporting Information Videos S4 and S5). The temporal evolution of the evaporating drop at 81 °C is given in Figures 12 and 13 at magnifications of 1000× and 100×, respectively (Supporting Information Videos S6 and S7). Similarly to the drying drop at 51 °C, a ringlike cluster can be observed at the top of the drop caused by the Marangoni effect (see Figures 11a-e and 13a-e). The Marangoni eddy identified previously at 51 °C is clearly shown between the edge and ringlike cluster by the dashed arrows in Figures 10b-h and 12a-g. As shown in insets in Figure 10g,h, the particles sorting near the edge is similar to that of the drying drop at 51 °C. However, unlike 51 °C, the depinning of the contact line prevents the ringlike cluster from reaching the initial contact line. The depinned

contact line pushes back the ringlike cluster toward the central regions of the drop (Figures 11f,g and 13f). Then, the ringlike cluster reaches the depinned contact line (Figures 11h and 13g), building a new distinctive ringlike structure in the drop center (Figures 11i and 13h,i). Subsequently, those particles trapped inside the ringlike cluster at the free interface deposit in the interior of the new ringlike structure, leading to the observed irregular distribution of particles there (see inside the secondary ring in Figures 11g-i and 13g-i). The formation mechanism of the inner ringlike structure deposited in the central region is schematized from the side view in Figure 9a,b,cII,dII,eII. Contrary to the what is observed for the case of 51 °C, the ringlike cluster did not reach the initial edge, and thus the rings (formed by 1 and 3.2 μm particles) in the edge region are distinctive (insets in Figures 10i and 12i). Figure S5 (in Supporting Information) shows that the depinning time of the initial contact line decreases with increasing temperature. Hence, at 51 °C, the depinning time is longer than that at higher temperatures. The longer depinning time at 51 °C leads to the arrival of the ringlike cluster to the edge region, and prevents from the formation of the secondary ringlike structure in the interior of the drop. However, the slightly earlier depinning at temperatures of 64 and 81 °C prevents from the arrival of the ringlike cluster to the edge, and hence the cluster deposits in the interior of the drop. In a similar manner to the heated case at 51 °C, a depleted zone (between the two bars in insets in Figures 10i and 12i) appears after the dry-out of the thin liquid film (shown between the two bars in inset in Figure 10g), which separates the ring built by 1 μm particles (marked as the middle ring in insets in Figures 10i and 12i) and the ring formed by particles smaller than 1 μm (marked as the outermost ring in Figures 10i and 12i). The innermost ring is formed by the mixture of both 1 and 3.2 μm particles (insets in Figures 10i and 12i). The depinning of the initial contact

line also pushes the innermost ring and consequently leads to the deformation or rupture of some parts of the ring (see the regions highlighted by the ovals in Figures 10f-i and 12f-i).

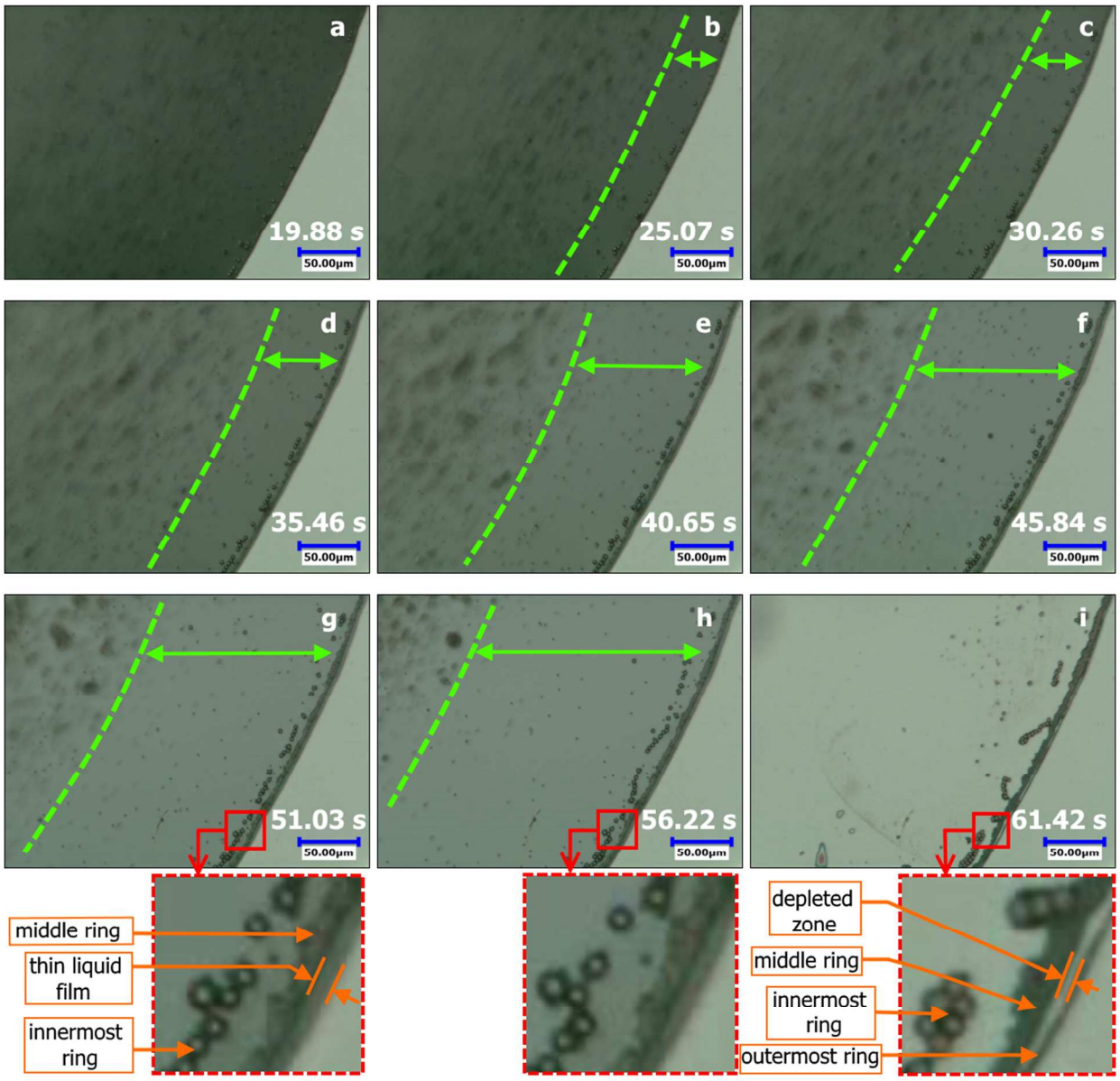

Figure 10. Snapshots from a video microscopy of the evaporation process of a 3 μL water-based bi-disperse drop containing a mixture of 3.2 μm diameter particles (mass concentration of 0.0125 wt %) and 1 μm mean diameter particles (mass concentration of 0.0125 wt %) onto a heated silicon substrate at 64 °C. The double arrows denote the eddy region between the ringlike cluster

and edge. Insets show the zoomed in regions highlighted in the solid rectangles. The micrographs are recorded at a temporal resolution of 125 fps and at 1000× magnification. Scale bars, 50 μm.

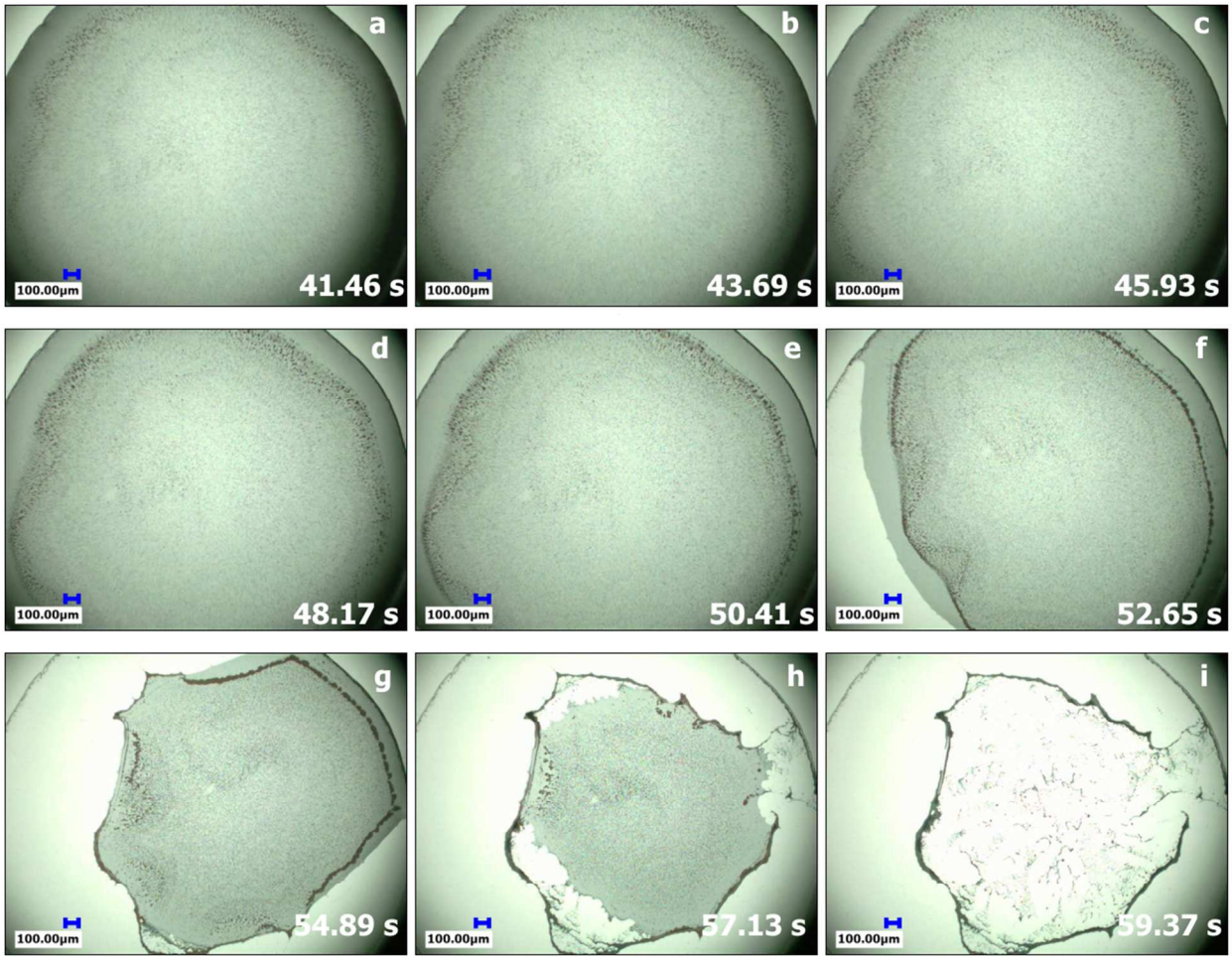

Figure 11. Snapshots from a video microscopy of the evaporation process of a 3 μL water-based bi-disperse drop containing a mixture of 3.2 μm diameter particles (mass concentration of 0.0125 wt %) and 1 μm mean diameter particles (mass concentration of 0.0125 wt %) onto a heated silicon substrate at 64 °C. The micrographs are recorded at a temporal resolution of 125 fps and at 100× magnification. Scale bars, 100 μm.

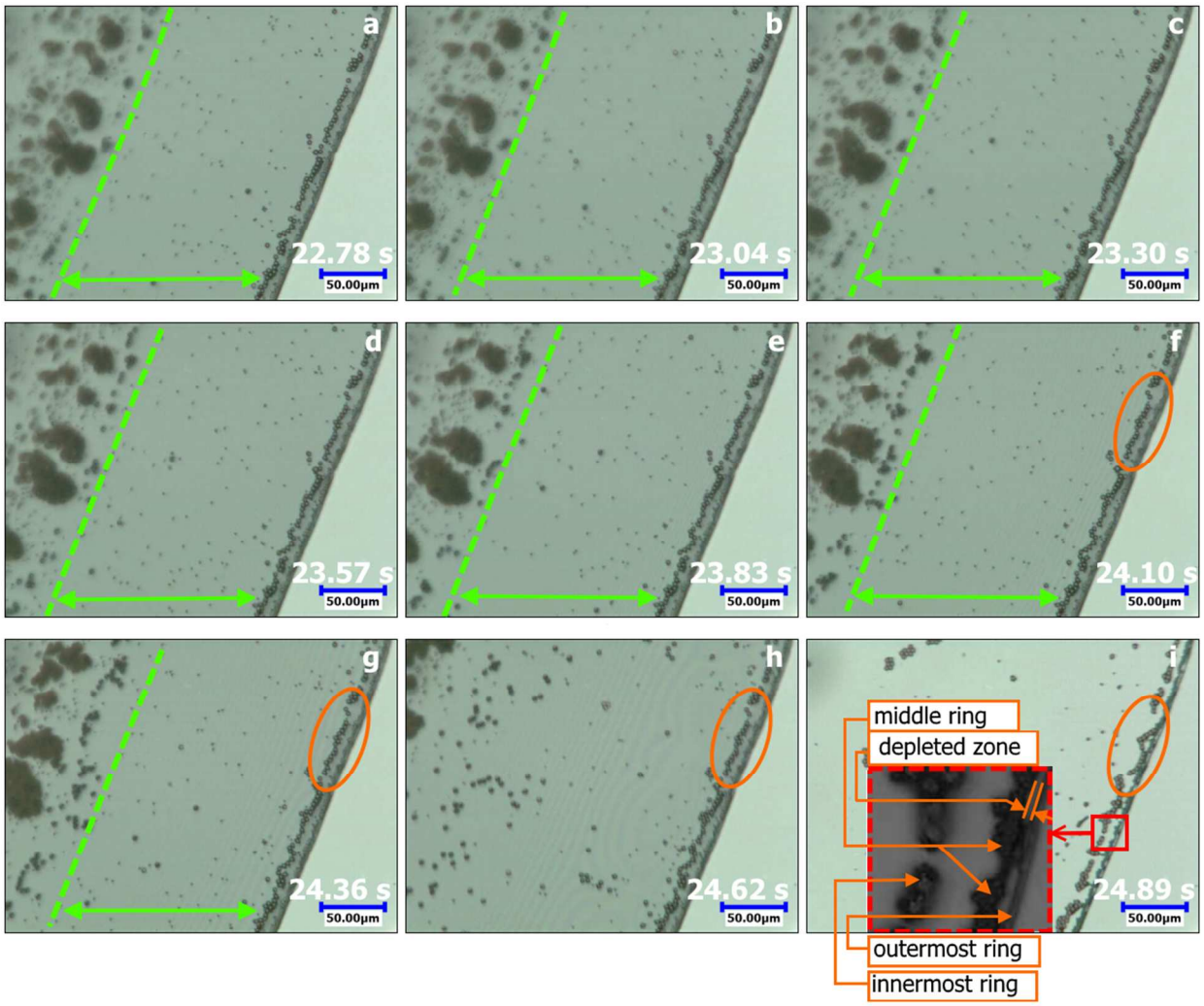

Figure 12. Snapshots from a video microscopy of the evaporation process of a 3 μL water-based bi-disperse drop containing a mixture of 3.2 μm diameter particles (mass concentration of 0.0125 wt %) and 1 μm mean diameter particles (mass concentration of 0.0125 wt %) onto a heated silicon substrate at 81 °C. The double arrows denote the eddy region between the ringlike cluster and edge. The micrographs are recorded at a temporal resolution of 125 fps and at 1000× magnification. Scale bars, 50 μm.

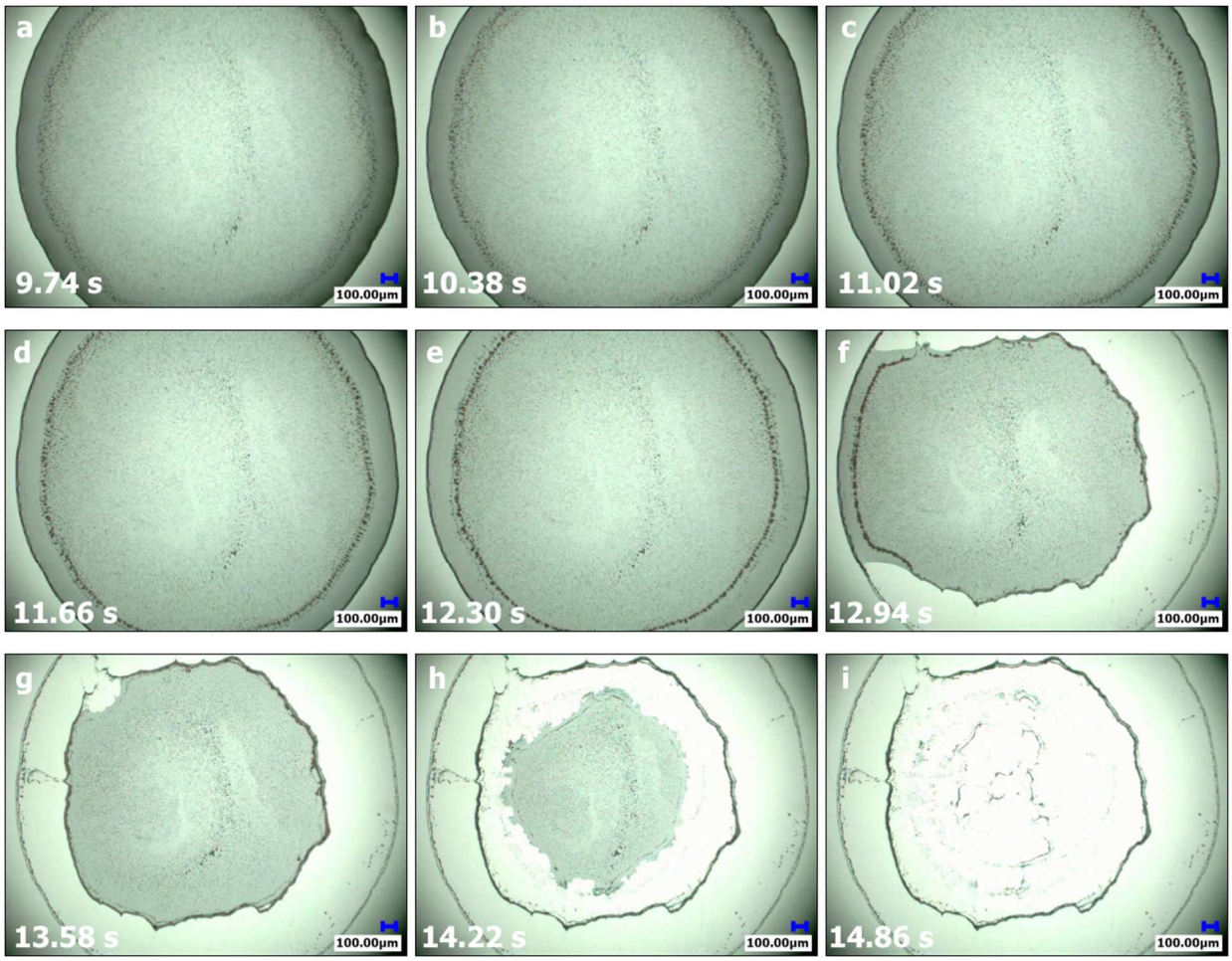

Figure 13. Snapshots from a video microscopy of the evaporation process of a 3 μL water-based bi-disperse drop containing a mixture of 3.2 μm diameter particles (mass concentration of 0.0125 wt %) and 1 μm mean diameter particles (mass concentration of 0.0125 wt %) onto a heated silicon substrate at 81 °C. The micrographs are recorded at a temporal resolution of 125 fps and at 100× magnification. Scale bars, 100 μm.

Figures 14 and 15 show top views of the drying drops at 99 °C at magnifications of 500× and 100×, respectively (Supporting Information Videos S8 and S9). The transportation of the particles participating in the eddy region can be observed due to the Marangoni effect (shown by the double arrows between the edge and dashed curve in Figure 14a-f). The ringlike cluster at the

top region of the drying drop is found to be identical to the drops evaporating at 64 and 81 °C (Figure 15a-c). In a similar manner to the droplets evaporating at 64 and 81 °C, the contact line depins before the ringlike cluster moving toward the edge (Figure 15d). The depinned contact line reaches the ringlike cluster, depositing it onto the substrate (Figure 15e). After that, the contact line jumps to a new position and remains pinned (Figure 15f,g). The contact line jumps for several times after each pinning stage (Figure 15g,h), leaving behind distinct deposition lines in the central region of the dried drop (Figure 15i). This evaporation process is known as the "stick-slip" behavior. The stick and slip of the contact line occurs from all sides of the drop (Figure 15d-h), leading to the formation of a "rose-like" pattern (Figures 15i and 16a). However, in some cases (at 99 °C), the typical "stick-slip" behavior is observed during which the contact line is pinned on one side of the drying drop (left side in Figure 16b), and it slips and sticks on the other side (right side of the drop in Figure 16b). Thus, the multiple concentric rings are formed with a preferential/initial pinning to one side, as shown in Figure 16b. That pinning of the contact line on one side of the droplet is (perhaps) due to irregularities on the surface.[54] A close examination of the initial contact line after the complete evaporation reveals that the observed outermost ring at lower temperatures (22, 51, 64 and 81 °C) almost overlaps the leading edge of the middle ring (see insets I in Figures 16a and 16b). Thus, the depleted zone between the contact line and the ring of 1 μm particles is not easily distinguishable (insets I in Figures 16a and 16b). There are two obvious rings of particles at the initial periphery of the dried drops (insets I in Figures 16a and 16b): one is the outermost ring, which is formed by 1 μm particles overlapping the non-volatile additives; and the other is the innermost ring which is built by the mixture of 1 and 3.2 μm particles. A magnified image of the initial contact line on the pinned side of the drop (inset II in Figure 16b) also shows the similar particle sorting but with larger

aggregation of 1 and 3.2 μm particles at the innermost ring which is due to the continuous pinning on that side of the drop during the evaporation. Inset II in Figure 16a and inset III in Figure 16b show the magnified pictures of the second deposition lines which are the remnants of the ringlike cluster deposited on the solid surface. Unlike the initial deposition line (shown by inset I in Figure 16a and insets I,II in Figure 16b), the second line consists of rings which are easily distinguishable from each other (inset II in Figure 16a and inset III in Figure 16b): the outermost ring formed by the non-volatile additives, the middle ring built by 1 μm particles, and the innermost ring formed by the mixture of all particle sizes. The width of the depleted zone is known to be a function of the geometric parameters (i.e., contact angle (θ), particle size (d_p)), and is relatively equal to $d_p/\tan\theta$ (see Figure 17).[34] As the width of the depleted zone is the distance between the initial contact line (or the outermost ring) and the ring of 1 μm particles (or middle ring), d_p should be equal to 1 μm and is constant for all studied cases. Thus, the width of the zone becomes larger with decreasing the contact angle (Figure 17). In other words, the larger the contact angle, the smaller becomes the zone. It is obvious that the initial contact angle of the drop at the initial contact line is larger than the contact angle (just after the first jump) at the second deposition line (see Figure 17aI,bI). Hence, the width of the zone at the initial contact line (inset I in Figure 16a and insets I,II in Figure 16b) is smaller than that at the second deposition line (inset II in Figure 16a and inset III in Figure 16b). Similarly, at 81 °C, the width at the initial deposition line is smaller compared to that at the inner ringlike structure (see Figure 17aII,bII). This is because the initial contact angle of the drop is larger than that of the drop at the deposition time of the ringlike cluster (see Figure 17aI,bI). As previously mentioned, several deposition lines are formed on the solid surface due to the "stick-slip" behavior. For the "rose-like" pattern, the structure of the other internal lines left by the "stick-slip" (apart from the

second line) are similar to what explained for the second deposition line (inset II in Figure 16a). However, the typical "stick-slip" deposit (Figure 16b) exhibits a different pattern (for the internal deposition lines) where there is a faint single ring connecting some triangular structures (see insets IV,V in Figure 16b). This can be attributed (perhaps) to the weak pinning of the contact line during the evaporation.[55] Thus, the retracting contact line carries the particles toward the pinned side of the drying drop and build these triangular structures.

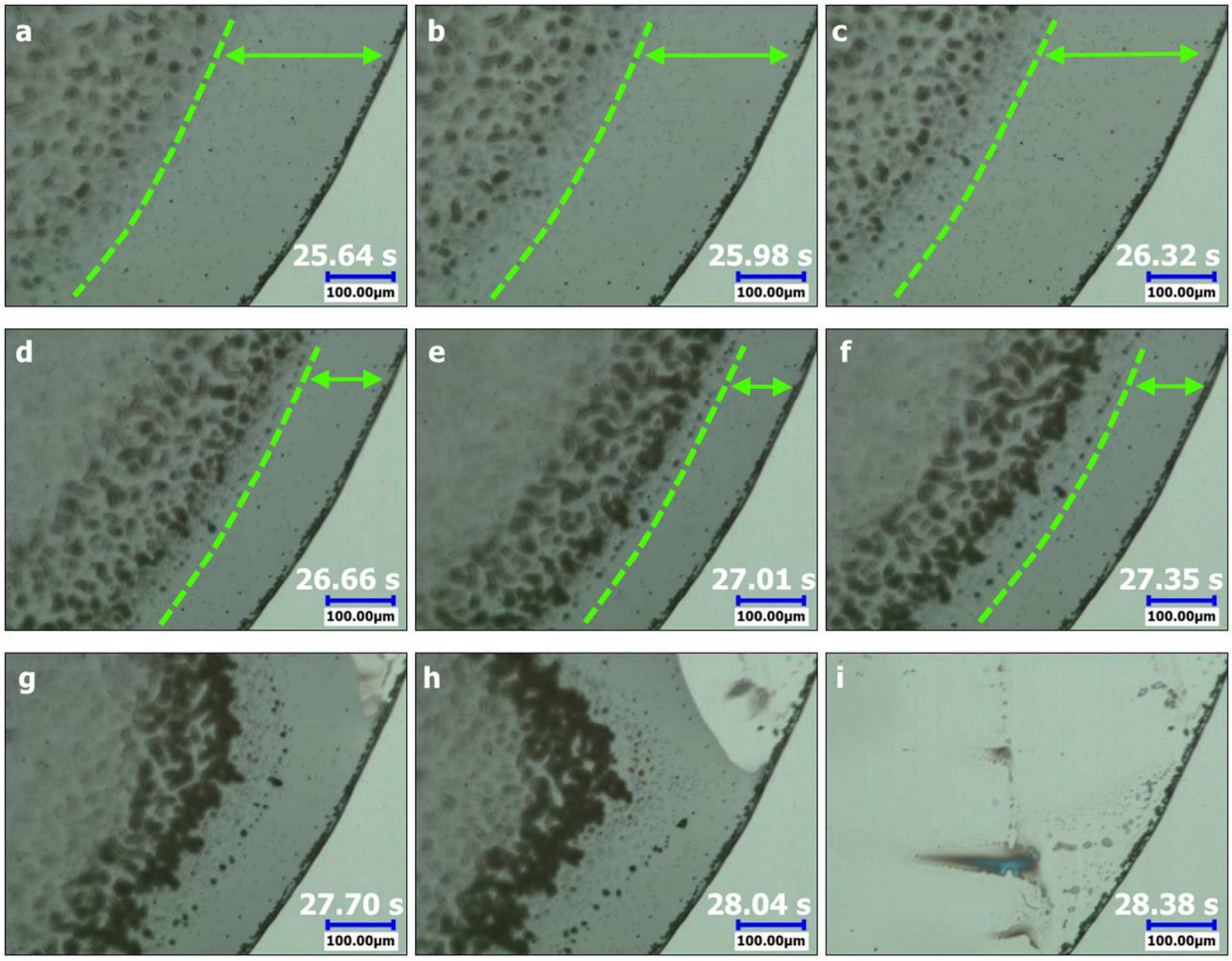

Figure 14. Snapshots from a video microscopy of the evaporation process of a 3 μL water-based bi-disperse drop containing a mixture of 3.2 μm diameter particles (mass concentration of 0.0125 wt %) and 1 μm mean diameter particles (mass concentration of 0.0125 wt %) onto a heated silicon substrate at 99 °C. The double arrows denote the eddy region between the ringlike cluster

and edge. The micrographs are recorded at a temporal resolution of 125 fps and at 500× magnification. Scale bars, 100 μm.

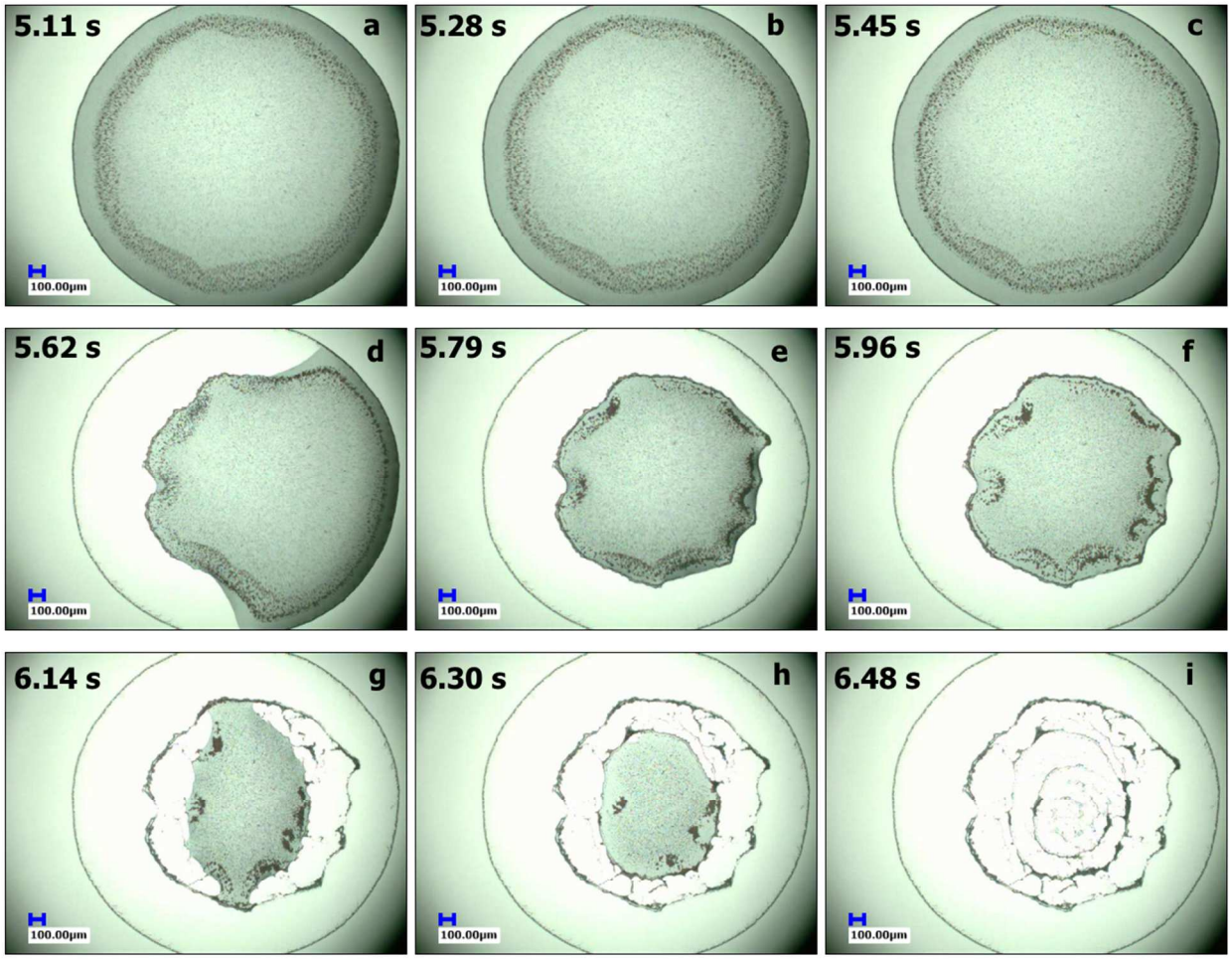

Figure 15. Snapshots from a video microscopy of the evaporation process of a 3 μL water-based bi-disperse drop containing a mixture of 3.2 μm diameter particles (mass concentration of 0.0125 wt %) and 1 μm mean diameter particles (mass concentration of 0.0125 wt %) onto a heated silicon substrate at 99 °C. The micrographs are recorded at a temporal resolution of 125 fps and at 100× magnification. Scale bars, 100 μm.

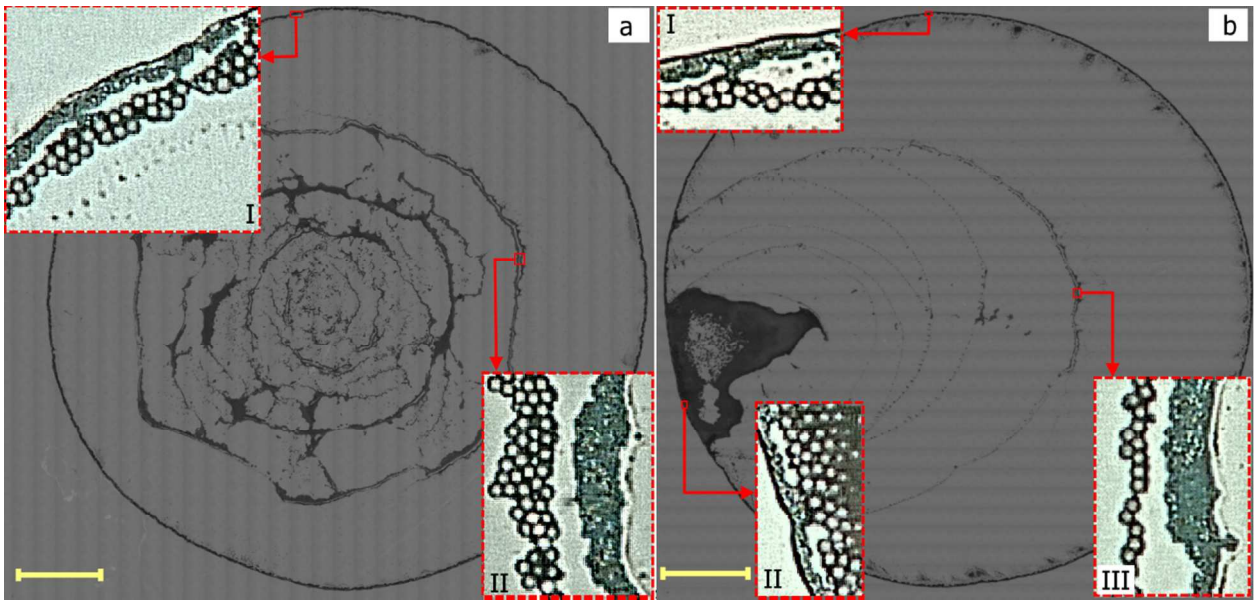

Figure 16. Dried deposits of bi-disperse drops containing a mixture of 3.2 μm diameter particles (mass concentration of 0.0125 wt %) and 1 μm mean diameter particles (mass concentration of 0.0125 wt %) onto a heated substrate at temperature of 99 °C: (a) The rose-like pattern - (I) initial contact line, and (II) the second deposition line. (b) The typical stick-slip pattern - (I) initial contact line on the depinned side, (II) initial contact line on the pinned side, (III) the second deposition line, (IV) the third deposition line, and (V) the fourth deposition line. Insets show the zoomed in regions highlighted in the solid rectangles. The initial volume of drops is: (a) 4.1, and (b) 5 μL. Scale bars, 600 μm.

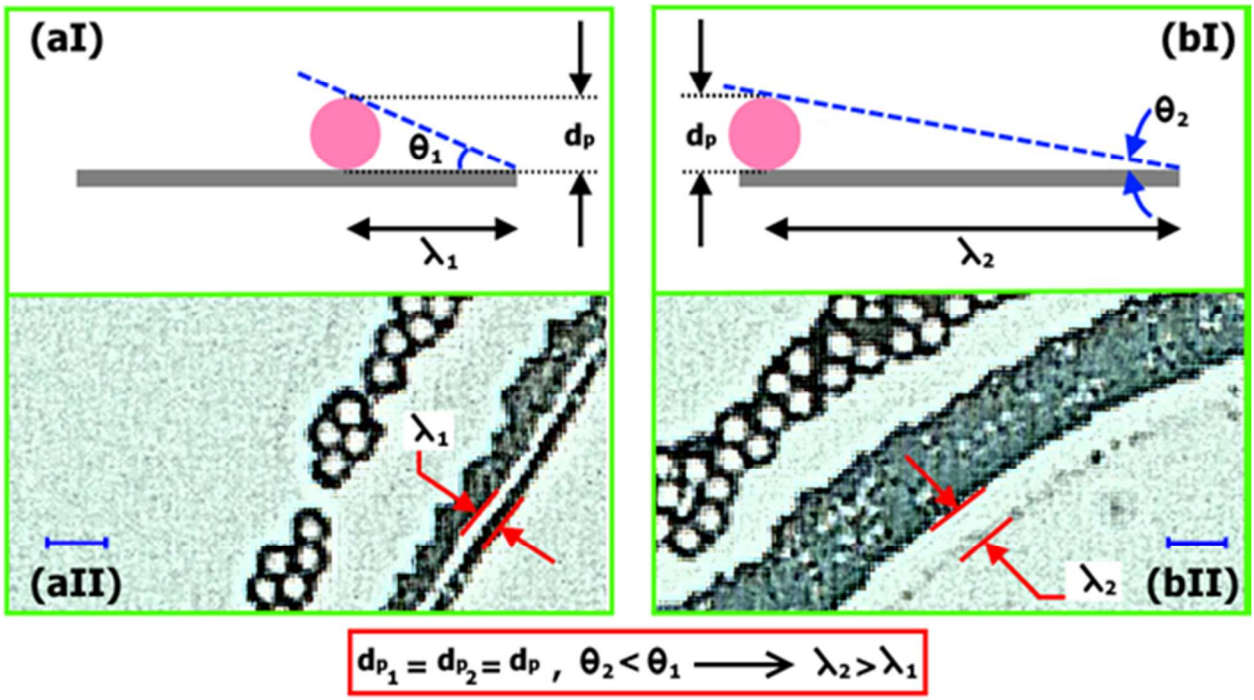

Figure 17. (aI) Schematic diagram of a 3 μL bi-dispersed drop's edge at the initial evaporation time. (aII) Particle sorting at the initial edge after the complete evaporation. (bI) Schematic diagram of the drop's edge at the deposition time of the ringlike cluster. (bII) Particle sorting after the deposition of the ringlike cluster. λ is the distance between the ring of non-volatile additives and the ring of 1 μm particles. θ is the contact angle. d_p is the diameter of the 1 μm particle. The drop contains a mixture of 3.2 μm diameter particles (mass concentration of 0.0125 wt %) and 1 μm mean diameter particles (mass concentration of 0.0125 wt %). Scale bars, 6 μm.

In studies related to the evaporation of monodispersed drops on heated substrates, the thermal Marangoni effect is the main mechanism behind the pattern formation of particles.[13] For monodispersed drops on heated substrates, the "dual-ring" pattern was observed for temperatures between 47 and 81 °C, but this pattern is not observed for bi-dispersed drops at temperature of 51 °C. Instead, a non-uniform deposition of particles enclosed by a thick ring is observed. This can be attributed to the different particle sorting near the contact line which (perhaps) affects the

depinning time, and thus the final deposition pattern. In the case of bi-dispersed drops at highest temperature of 99 °C, two different patterns from the "stick-slip" behavior are observed, whereas only one particular pattern (similar to sample VI in Figure 1b) was reported after the stick-slip behavior for monodispersed drops.[13] Overall, the final deposition pattern of bi-dispersed drops on heated substrates is significantly dependent on the thermal Marangoni effect rather than the particle size effect. However, the size effect plays an important role in the deposition pattern of the regions near the contact line, and it is quite different from the monodispersed cases.

Particle Velocity. The particle velocity is measured at the distance of 50 μm from the contact line and presented as a function of normalized time in Figure 18. It should be noted that only those particles deposit at near the edge are considered for this measurement. In other words, the particles inside the outward flow region are tracked for the measurement of velocity (see solid arrows in Figure 8). Hence, the repelled particles in the Marangoni flow region are not included in this measurement (see dashed arrows in Figure 8). Using the models by Deegan et al.,[11] the theoretical height-averaged velocity is calculated close to the contact line which is given by[47]

$$\tilde{u}(r,t) = \frac{R}{4\left(\frac{r}{R}\right)(t_e - t)}\left(\frac{1}{\sqrt{1-\left(\frac{r}{R}\right)^2}} - \left[1-\left(\frac{r}{R}\right)^2\right]\right) \quad (1)$$

where R is the drop radius; r, the distance from the drop center; t, the evaporation time; and t_e, the total evaporation time. For the plots in Figure 18, the value of r is equal to the difference between the drop radius and the distance of measurements from the contact line ($r = R - 50$ μm). As it can be seen in Figure 18, both the experimental and theoretical velocities gradually increase with time, but they increase abruptly at the last stages of the evaporation. This sudden change in the velocity is known as the "rush-hour" behavior.[46,47] The observation of the rush-hour behavior has been reported previously for drying drops on nonheated substrates.[46,47] Here,

the similar behavior is observed for evaporating bi-dispersed drops on both nonheated and heated substrates. The outward flow towards the contact line is generated to replenish the evaporated liquid while the drop height is vanishing with the evaporation time. Thus, the liquid is squeezed through the vanishing area, leading to a diverging radial velocity. The critical time at which the radial velocity diverges is indicated by the dashed line which is estimated between the normalized time of 0.7 and 0.8 for all temperatures between 22 and 81 °C (Figure 18). Despite the trend of the theoretical velocity matches well with the experimental one, there is a difference between the measured and calculated values. This discrepancy can be attributed to the distance between the objective lens and substrate for experimental measurements which is not considered in the model. In addition, the increase of temperature changes the properties of the liquid and vapor (i.e., liquid density, vapor concentration, vapor diffusivity) and it is also not included in the model. Marín et al.[46] introduced a more developed model to calculate the theoretical height-averaged velocity which includes all abovementioned and other extra parameters (i.e., contact angle, height). However, it cannot be used in this study as the simultaneous side view and top view visualizations of drops were not possible.

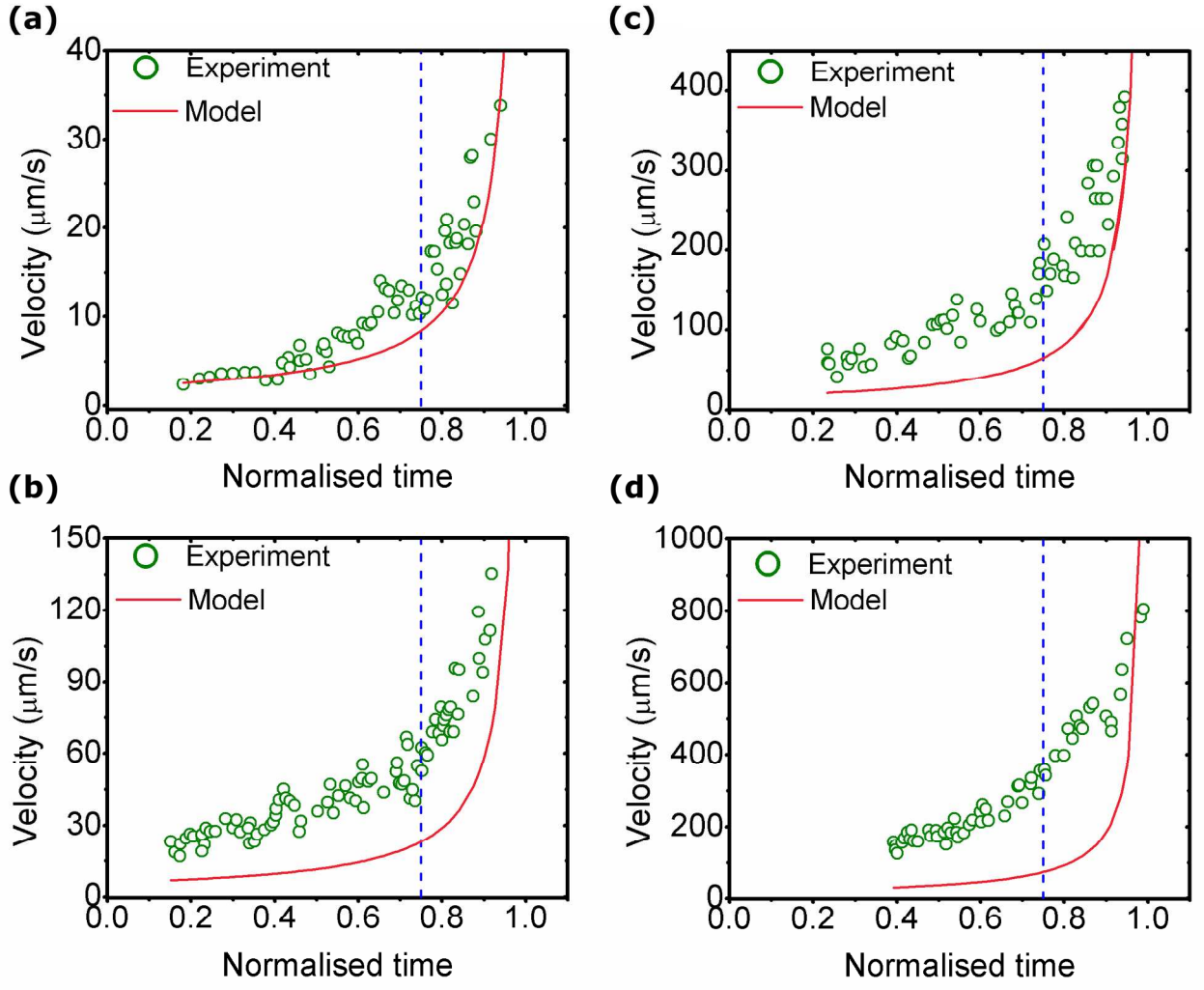

Figure 18. Particle velocity versus normalized time for drying 3 μL bi-dispersed drops containing a mixture of 3.2 μm diameter particles (mass concentration of 0.0125 wt %) and 1 μm mean diameter particles (mass concentration of 0.0125 wt %) onto heated substrates at: (a) 22 °C, (b) 51 °C, (c) 64 °C, and (d) 81 °C. The dashed line indicates the start of the rush-hour behavior.

Location of Stagnation Point. To determine the location of the stagnation point in evaporating bi-dispersed drops onto heated substrates, the 1 μm particles are tracked and the turning points of these particles returning back to the top surface of the drops are shown by the crosses in Figure 19. The crosses show that the particles can change the direction in different

distances from the contact line. During the entire evaporation of drops at 51 and 64 °C, the nearest turning points to the contact line are found to be adjacent to the ring of 3.2 μm particles (innermost ring) (see insets in Figure 19a,b). On the other hand, it is observed that those other particles that reach the region between the innermost ring and the ring of 1 μm particles do not turn back, and finally deposit at the ring of 1 μm (middle ring). These observations reveal that the distance between the stagnation point and the contact line (the so-called stagnation distance) is smaller than that between the innermost ring and contact line, thus the stagnation point should be located somewhere between the innermost and the middle rings (for evaporating drops at 51 and 64 °C). At substrate temperature of 81 °C, the nearest turning point to the contact line is observed between the innermost and middle rings (see inset in Figure 19c). Hence, at 81 °C, the stagnation point should be in the immediate vicinity of the middle ring. The measured distances between the nearest turning point and the contact line are approximately 11, 9, and 7 μm for substrate temperatures of 51, 64, and 81 °C, respectively. This shows that increasing the substrate temperature decreases the stagnation distance within drying bi-dispersed drops. This observation is in a good agreement with the study of Li et al.[42] who showed that the stagnation distance decreased with the substrate temperature inside evaporating monodispersed drops. However, a more detailed study is required to estimate the stagnation distance by considering the effect of geometrical parameters (i.e., contact angle). For example, the initial contact angle of the drop affects the width of the thin liquid film between the initial contact line and the middle ring, which may have influence on the stagnation distance. In other words, the larger width of the thin liquid film may increase the stagnation distance, and vice versa.

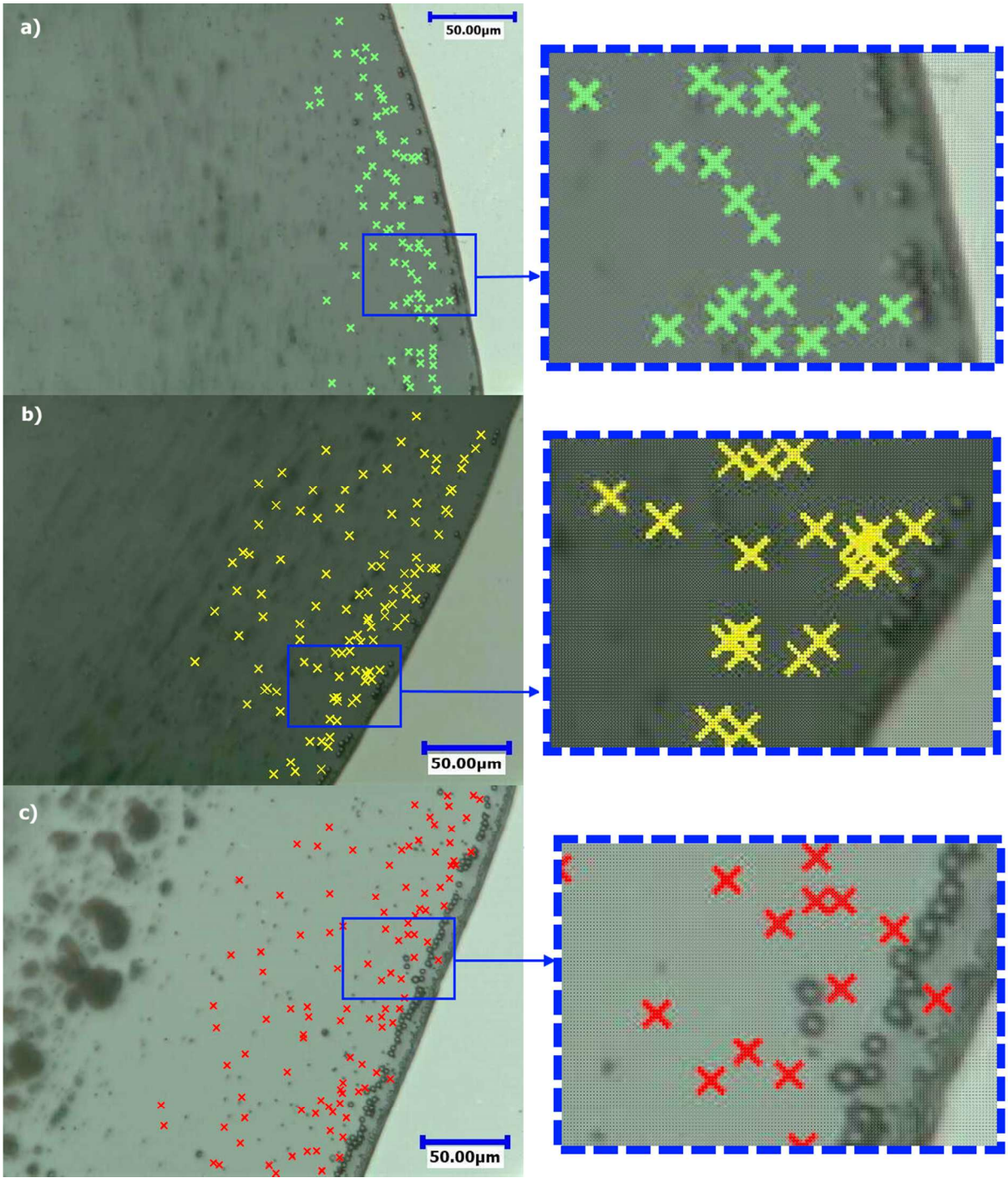

Figure 19. Turning points of 1 μm particles are shown by the crosses inside 3 μL bi-dispersed drops containing a mixture of 3.2 μm diameter particles (mass concentration of 0.0125 wt %) and 1 μm mean diameter particles (mass concentration of 0.0125 wt %) onto heated substrates at: (a)

51 °C, (b) 64 °C, and (c) 81 °C. Insets show the zoomed in regions highlighted in the solid rectangles.

CONCLUSION

In summary, the results of the deposition patterns from evaporating bi-dispersed drops onto both nonheated and heated silicon substrates were reported. On nonheated substrate, a nearly uniform deposition pattern enclosed by the disk-like ring was observed. On heated substrates, the inward thermal Marangoni flow formed a ringlike cluster of particles on the top surface of the drops, which had a significant role in the final deposition patterns. The internal flow was divided into two regions of the outward "coffee-ring" flow and the Marangoni flow by a stagnation point where the flow changed its direction. At the substrate temperature of 51 °C, the ringlike cluster reached the initial edge just before the depinning of the contact line, and thus a relatively non-uniform deposition pattern enclosed by the thick ring was formed. From temperatures from 64 to 81 °C, the depinning of the initial contact line occurred before the arrival of the ringlike cluster toward the edge, forming a ringlike structure on the surface. Hence, a "dual-ring" pattern was left after the full evaporation: one is the ringlike structure at the periphery; the other is the inner ringlike structure left by the cluster. However, at 99 °C, the stick-slip behavior of the contact line led to the formation of a "stick-slip" pattern. Magnification at the drops edge showed three rings in the regions near the contact line after the complete evaporation: one was the outermost ring formed by the non-volatile additives smaller than 1 μm; the second was the middle ring formed by the 1 μm particles; and, the other is the innermost ring formed by the mixture of 1 and 3.2 μm particles. However, at some cases, the outermost ring was found to be nearly overlapped the middle ring. The width of the zone between the outermost ring and the middle ring was shown to be different at the initial edge and the edge of the inner ringlike structure (for temperatures from

64 to 99 °C). The width of the zone at the initial edge was found to be smaller than that at the edge of the inner ringlike structure. This was explained by the difference between the values of the contact angles at the initial time and the deposition time of the inner ringlike structure. Furthermore, velocity of small particles was measured and compared with a theoretical model. The theoretical trend fitted well with the experimental one, but there was a discrepancy between the theoretical and experimental values. Particle velocity slightly increased with time but it rapidly increased at the last stages of the evaporation, known as the "rush-hour" behavior. At all examined temperatures, the "rush-hour" behavior began between the normalized times of 0.7 and 0.8. Moreover, the 1 μm particles were tracked during the evaporation, and the nearest position of the turning point of tracer particles was found. For the substrate temperatures of 51 and 64 °C, the nearest turning point was observed adjacent to the innermost ring. However, the nearest turning point at 81 °C was found to be between the innermost and middle rings. By comparing the distance between the nearest turning points and the contact line for the temperatures of 51, 64 and 81 °C, it was found that increasing the substrate temperature decreased the stagnation distance.

AUTHOR INFORMATION

Corresponding Author

*Email: souad.harmand@univ-valenciennes.fr

Author Contributions

All authors contributed to the design of the experiments. M.P. performed the experiments, and analyzed the data with support from S.H. and K.S.; M.P. wrote the manuscript with support from

S.H. and K.S.; R.D. is responsible for the scan of the silicon wafers by means of the white light interferometer. M.B. is responsible for the characterization of the particle deposits shown in Figures S2-S4 in Supporting Information. All authors have given approval to the final version of the manuscript.

ACKNOWLEDGMENT

This work has been achieved within the framework of CE2I project (Convertisseur d'Énergie Intégré Intelligent). CE2I is co-financed by European Union with the financial support of European Regional Development Fund (ERDF), French State and the French Region of Hauts-de-France.

ASSOCIATED CONTENT

Supporting Information

Microscopic videos of the evaporating bi-dispersed droplets at all substrate temperatures. Topography of the particle deposits and density distribution of particles at all substrate temperatures. Normalized depinning time of the bi-dispersed droplets versus temperature. This material is available free of charge via the Internet at http://pubs.acs.org.

REFERENCES

(1) Bermel, A. D.; Bugner, D. E. Particle Size Effects in Pigmented Ink Jet Inks. *J. Imaging Sci. Technol.* **1999**, *43* (4), 320–324.

(2) Sowade, E.; Blaudeck, T.; Baumann, R. R. Inkjet Printing of Colloidal Nanospheres: Engineering the Evaporation-Driven Self-Assembly Process to Form Defined Layer

Morphologies. *Nanoscale Res. Lett.* **2015**, *10* (1), 362.

(3) Kawase, T.; Sirringhaus, H.; Friend, R. H.; Shimoda, T. Inkjet Printed via-Hole Interconnections and Resistors for All-Polymer Transistor Circuits. *Adv. Mater.* **2001**, *13* (21), 1601–1605.

(4) De Gans, B. J.; Duineveld, P. C.; Schubert, U. S. Inkjet Printing of Polymers: State of the Art and Future Developments. *Adv. Mater.* **2004**, *16* (3), 203–213.

(5) Harris, D. J.; Hu, H.; Conrad, J. C.; Lewis, J. A. Patterning Colloidal Films via Evaporative Lithography. *Phys. Rev. Lett.* **2007**, *98* (14), 148301.

(6) Choi, Y.; Han, J.; Kim, C. Pattern Formation in Drying of Particle-Laden Sessile Drops of Polymer Solutions on Solid Substrates. *Korean J. Chem. Eng.* **2011**, *28* (11), 2130–2136.

(7) Xia, Y.; Gates, B.; Li, Z.-Y. Self-Assembly Approaches to Three-Dimensional Photonic Crystals. *Adv. Mater.* **2001**, *13* (6), 409–413.

(8) Chen, R.; Zhang, L.; Zang, D.; Shen, W. Blood Drop Patterns: Formation and Applications. *Adv. Colloid Interface Sci.* **2016**, *231*, 1–14.

(9) Brutin, D.; Sobac, B.; Loquet, B.; Sampol, J. Pattern Formation in Drying Drops of Blood. *J. Fluid Mech.* **2011**, *667*, 85–95.

(10) Deegan, R. D.; Bakajin, O.; Dupont, T. F.; Huber, G.; Nagel, S. R.; Witten, T. A. Capillary Flow as the Cause of Ring Stains from Dried Liquid Drops. *Nature* **1997**, *389* (6653), 827–829.

(11) Deegan, R.; Bakajin, O.; Dupont, T.; Huber, G.; Nagel, S.; Witten, T. Contact Line

Deposits in an Evaporating Drop. *Phys. Rev. E* **2000**, *62* (1), 756–765.

(12) Hu, H.; Larson, R. G. Marangoni Effect Reverses Coffee-Ring Depositions. *J. Phys. Chem. B* **2006**, *110* (14), 7090–7094.

(13) Parsa, M.; Harmand, S.; Sefiane, K.; Bigerelle, M.; Deltombe, R. Effect of Substrate Temperature on Pattern Formation of Nanoparticles from Volatile Drops. *Langmuir* **2015**, *31* (11), 3354–3367.

(14) Hu, Y.-C.; Zhou, Q.; Ye, H.-M.; Wang, Y.-F.; Cui, L.-S. Peculiar Surface Profile of Poly(ethylene Oxide) Film with Ring-like Nucleation Distribution Induced by Marangoni Flow Effect. *Colloids Surfaces A Physicochem. Eng. Asp.* **2013**, *428*, 39–46.

(15) Askounis, A.; Sefiane, K.; Koutsos, V.; Shanahan, M. E. R. The Effect of Evaporation Kinetics on Nanoparticle Structuring within Contact Line Deposits of Volatile Drops. *Colloids Surfaces A Physicochem. Eng. Asp.* **2014**, *441*, 855–866.

(16) Brutin, D. Influence of Relative Humidity and Nano-Particle Concentration on Pattern Formation and Evaporation Rate of Pinned Drying Drops of Nanofluids. *Colloids Surfaces A Physicochem. Eng. Asp.* **2013**, *429*, 112–120.

(17) Orejon, D.; Sefiane, K.; Shanahan, M. E. R. Evaporation of Nanofluid Droplets with Applied DC Potential. *J. Colloid Interface Sci.* **2013**, *407*, 29–38.

(18) Eral, H. B.; Augustine, D. M.; Duits, M. H. G.; Mugele, F. Suppressing the Coffee Stain Effect: How to Control Colloidal Self-Assembly in Evaporating Drops Using Electrowetting. *Soft Matter* **2011**, *7* (10), 4954.

(19) Zhong, X.; Duan, F. Evaporation of Sessile Droplets Affected by Graphite Nanoparticles

and Binary Base Fluids. *J. Phys. Chem. B* **2014**, *118* (47), 13636–13645.

(20) Zhong, X.; Duan, F. Flow Regime and Deposition Pattern of Evaporating Binary Mixture Droplet Suspended with Particles. *Eur. Phys. J. E* **2016**, *39* (2), 18.

(21) Still, T.; Yunker, P. J.; Yodh, A. G. Surfactant-Induced Marangoni Eddies Alter the Coffee-Rings of Evaporating Colloidal Drops. *Langmuir* **2012**, *28* (11), 4984–4988.

(22) Sempels, W.; De Dier, R.; Mizuno, H.; Hofkens, J.; Vermant, J. Auto-Production of Biosurfactants Reverses the Coffee Ring Effect in a Bacterial System. *Nat. Commun.* **2013**, *4*, 1757.

(23) Crivoi, A.; Duan, F. Effect of Surfactant on the Drying Patterns of Graphite Nanofluid Droplets. *J. Phys. Chem. B* **2013**, *117* (19), 5932–5938.

(24) Yunker, P. J.; Still, T.; Lohr, M. A.; Yodh, A. G. Suppression of the Coffee-Ring Effect by Shape-Dependent Capillary Interactions. *Nature* **2011**, *476* (7360), 308–311.

(25) Chon, C. H.; Paik, S.; Tipton, J. B.; Kihm, K. D. Effect of Nanoparticle Sizes and Number Densities on the Evaporation and Dryout Characteristics for Strongly Pinned Nanofluid Droplets. *Langmuir* **2007**, *23* (6), 2953–2960.

(26) Lee, H. H.; Fu, S. C.; Tso, C. Y.; Chao, C. Y. H. Study of Residue Patterns of Aqueous Nanofluid Droplets with Different Particle Sizes and Concentrations on Different Substrates. *Int. J. Heat Mass Transf.* **2017**, *105*, 230–236.

(27) Huang, J.; Kim, F.; Tao, A. R.; Connor, S.; Yang, P. Spontaneous Formation of Nanoparticle Stripe Patterns through Dewetting. *Nat. Mater.* **2005**, *4* (12), 896–900.

(28) Jung, J. Y.; Kwak, H. Y. Separation of Microparticles and Biological Cells inside an Evaporating Droplet Using Dielectrophoresis. *Anal. Chem.* **2007**, *79* (13), 5087–5092.

(29) Erb, R. M.; Son, H. S.; Samanta, B.; Rotello, V. M.; Yellen, B. B. Magnetic Assembly of Colloidal Superstructures with Multipole Symmetry. *Nature* **2009**, *457* (7232), 999–1002.

(30) Jung, J.-Y.; Kim, Y. W.; Yoo, J. Y. Behavior of Particles in an Evaporating Didisperse Colloid Droplet on a Hydrophilic Surface. *Anal. Chem.* **2009**, *81* (19), 8256–8259.

(31) Sangani, A. S.; Lu, C.; Su, K.; Schwarz, J. A. Capillary Force on Particles near a Drop Edge Resting on a Substrate and a Criterion for Contact Line Pinning. *Phys. Rev. E* **2009**, *80* (1), 11603.

(32) Weon, B. M.; Je, J. H. Capillary Force Repels Coffee-Ring Effect. *Phys. Rev. E* **2010**, *82* (1), 15305.

(33) Chhasatia, V. H.; Sun, Y. Interaction of Bi-Dispersed Particles with Contact Line in an Evaporating Colloidal Drop. *Soft Matter* **2011**, *7* (21), 10135–10143.

(34) Monteux, C.; Lequeux, F. Packing and Sorting Colloids at the Contact Line of a Drying Drop. *Langmuir* **2011**, *27* (6), 2917–2922.

(35) Wong, T. S.; Chen, T. H.; Shen, X.; Ho, C. M. Nanochromatography Driven by the Coffee Ring Effect. *Anal. Chem.* **2011**, *83* (6), 1871–1873.

(36) Devlin, N. R.; Loehr, K.; Harris, M. T. The Importance of Gravity in Droplet Evaporation: A Comparison of Pendant and Sessile Drop Evaporation with Particles. *AIChE J.* **2016**, *62* (3), 947–955.

(37) Devlin, N. R.; Loehr, K.; Harris, M. T. The Separation of Two Different Sized Particles in an Evaporating Droplet. *AIChE J.* **2015**, *61* (10), 3547–3556.

(38) Zhong, X.; Xie, H.; Duan, F. Deposition Patterns from Evaporating Sessile Droplets with Suspended Mixtures of Multi-Sized and Multi-Species Hydrophilic and Non-Adsorbing Nanoparticles. *Appl. Therm. Eng.* **2017**, *111*, 1565–1572.

(39) Han, W.; Byun, M.; Lin, Z. Assembling and Positioning Latex Nanoparticles via Controlled Evaporative Self-Assembly. *J. Mater. Chem.* **2011**, *21* (42), 16968.

(40) Jeong, H.; van Tiem, J.; Gianchandani, Y. B.; Park, J. Nano-Particle Separation Using Marangoni Flow in Evaporating Droplets. In *Solid-State Sensors, Actuators and Microsystems Workshop*; Hilton Head Island, 2014; pp 223–226.

(41) Hendarto, E.; Gianchandani, Y. B. Size Sorting of Floating Spheres Based on Marangoni Forces in Evaporating Droplets. *J. Micromechanics Microengineering* **2013**, *23* (7), 75016.

(42) Li, Y.; Lv, C.; Li, Z.; Quéré, D.; Zheng, Q. From Coffee Rings to Coffee Eyes. *Soft Matter* **2015**, *11* (23), 4669–4673.

(43) Patil, N. D.; Bange, P. G.; Bhardwaj, R.; Sharma, A. Effects of Substrate Heating and Wettability on Evaporation Dynamics and Deposition Patterns for a Sessile Water Droplet Containing Colloidal Particles. *Langmuir* **2016**, *32* (45), 11958–11972.

(44) Zhong, X.; Duan, F. Disk to Dual Ring Deposition Transformation in Evaporating Nanofluid Droplets from Substrate Cooling to Heating. *Phys. Chem. Chem. Phys.* **2016**, *18* (30), 20664–20671.

(45) Zhong, X.; Wu, C.; Duan, F. From Enhancement to Elimination of Dual-Ring Pattern of Nanoparticles from Sessile Droplets by Heating the Substrate. *Appl. Therm. Eng.* **2017**, *115*, 1418–1423.

(46) Marín, Á. G.; Gelderblom, H.; Lohse, D.; Snoeijer, J. H. Order-to-Disorder Transition in Ring-Shaped Colloidal Stains. *Phys. Rev. Lett.* **2011**, *107* (8), 85502.

(47) Marín, Á. G.; Gelderblom, H.; Lohse, D.; Snoeijer, J. H. Rush-Hour in Evaporating Coffee Drops. *Phys. Fluids* **2011**, *23* (9), 91111.

(48) Kralchevsky, P. A.; Denkov, N. D. Capillary Forces and Structuring in Layers of Colloid Particles. *Curr. Opin. Colloid Interface Sci.* **2001**, *6* (4), 383–401.

(49) Di Leonardo, R.; Saglimbeni, F.; Ruocco, G. Very-Long-Range Nature of Capillary Interactions in Liquid Films. *Phys. Rev. Lett.* **2008**, *100* (10), 106103.

(50) Xu, X.; Luo, J. Marangoni Flow in an Evaporating Water Droplet. *Appl. Phys. Lett.* **2007**, *91* (12), 124102.

(51) Parsa, M.; Boubaker, R.; Harmand, S.; Sefiane, K.; Bigerelle, M.; Deltombe, R. Patterns from Dried Water-Butanol Binary-Based Nanofluid Drops. *J. Nanoparticle Res.* **2017**, *19* (8), 268.

(52) Xu, X.; Ma, L.; Huang, D.; Luo, J.; Guo, D. Linear Growth of Colloidal Rings at the Edge of Drying Droplets. *Colloids Surfaces A Physicochem. Eng. Asp.* **2014**, *447*, 28–31.

(53) Parsa, M.; Harmand, S.; Sefiane, K.; Bigerelle, M. Evaporation of Binary Mixture Nanofluid Drops: Pattern Formation. In *10th Annual TechConnect World Innovation Conference*; Laudon, M., Case, F., Romanowicz, B., Eds.; TechConnect: Washington,

2016; Vol. 3, pp 196–197.

(54) Orejon, D. A Study of Nanosuspension Droplets Free Evaporation and Electrowetting, University of Edinburgh, 2013.

(55) Askounis, A.; Sefiane, K.; Koutsos, V.; Shanahan, M. E. R. Effect of Particle Geometry on Triple Line Motion of Nano-Fluid Drops and Deposit Nano-Structuring. *Adv. Colloid Interface Sci.* **2015**, *222*, 44–57.

Table of Contents Graphic